PRACTICAL CONSIDERATIONS FOR RADAR EMBEDDED COMMUNICATION

by

Casey Biggs

Submitted to the graduate degree program in Electrical Engineering & Computer Science and the Graduate Faculty of the University of Kansas School of Engineering in partial fulfillment of the requirements for the degree of Master of Science.

Thesis Committee:

_____
Dr. Shannon D. Blunt (Chair)

_____
Dr. Christopher Allen

_____
Dr. Erik Perrins

1st July 2009
Date of Thesis Defense

The thesis committee for Casey Biggs certifies that

this is the approved version of the following thesis:

PRACTICAL CONSIDERATIONS FOR RADAR EMBEDDED COMMUNICATION

Dr. Shannon D. Blunt (Chair)

Dr. Christopher Allen

Dr. Erik Perrins

1st July 2009

Date Approved

Acknowledgements

I would first like to thank my advisor Dr. Shannon Blunt for his continued guidance and support in understanding and advancing this research and writing this thesis. I would like to thank the Air Force Office of Scientific Research (AFOSR) for sponsoring the research. Special thanks to Dr. Christopher Allen and Dr. Erik Perrins for agreeing to be on my thesis committee. I would also like to thank my professors and classmates for making my return to school enjoyable. Last, but not least, I would like to thank my family and friends for their support through this busy time.

Table of Contents

Abstract

This thesis expands on the previous work done in the area of intra-pulse radar embedded communication by examining some of the practical aspects of the waveform design. Communication waveform mismatches between the tag and receiver due to multipath distortion, sampling rate differences and using different lengths for the radar waveform are explored for each of the three previously developed design methods. The Dominant-Projection approach is shown to be robust to most mismatches while the other two approaches significantly degrade or fail with any mismatch. Lack of synchronization between the receiver and tag is shown to increase the occurrence of symbol errors, since the receiver is required to search over multiple samples for the communication waveform sent by the tag. Attempts to reduce the number of errors caused by the lack of synchronization are also made, first by taking a three sample average of the filter output and second by generating waveforms with lower local cross-correlation, with both attempts shown to be unsuccessful. Other attempts are also made to improve the waveform design. It is shown that temporal expansion can be used to either improve symbol error rate or reduce the amount of bandwidth expansion required. A rule-of-thumb is developed for the bandwidth expansion versus temporal expansion trade-off. It is also shown that more of the dominant space can be projected out with Dominant-Projection to reduce the probability of symbol error, but this comes at the cost of being more susceptible to being detected by an intercept receiver.

CHAPTER 1

INTRODUCTION

The ability to communicate without interception can at times be highly desirable, especially in military applications. Previously, systems have been deployed that embed communication signals into the backscatter of radar by operating on a pulse to pulse basis to achieve covert communication, but at a low data rate. Previous work in [1]-[4] develops symbol waveforms that work instead on an intra-pulse basis to achieve a higher data rate than the inter-pulse methods while still remaining covert. In this thesis, some of the practical aspects of an intra-pulse radar embedded communication system are discussed and the three symbol waveform designs are tested to see how they perform in more real world situations. Also, the communication waveform design is explored and modified in an attempt to reduce the symbol error rate (SER) while maintaining a low probability of intercept (LPI).

In a radar system, a transmitter sends out a radio frequency (RF) signal (pulsed or continuous) that scatters off objects that it encounters. A receiver collects the scattered signal to determine information (range, velocity, cross-section, etc.) about the illuminated objects [5]. An RF tag/transponder that is illuminated by the radar can embed a communication signal in its backscatter by remodulating the incident waveform. To be effective, the communication waveforms need to be similar enough to the ambient scattering of the radar signal to be difficult to intercept, yet separable enough from the clutter to be detected by an intended receiver with a low

probability of symbol error.

Three design methods were previously developed to generate the symbol waveforms for intra-pulse communication. Each method utilizes that the spectrum of most radar signals spread out beyond their passband. This “bleeding” spectrum of the radar waveform is used as expanded bandwidth for the communication waveforms to reside. Also, each method uses the eigenvectors from a correlation matrix based on the ambient scattering of the radar signal to produce communication waveforms that are partially correlated with the clutter in an effort to be more hidden.

1.1 MOTIVATION OF THESIS

The motivation of this thesis is to examine some of the practical aspects of intra-pulse radar embedded communication when using the three previously developed waveform design approaches in [1]-[4]. Also, attempts to improve waveform and receiver design are explored in order to achieve a higher symbol error rate and/or to have the communication signal be more hidden and thus have a lower probability of intercept.

Each of the communication waveform design methods use the incident radar signal at the tag in the symbol generation process to produce waveforms that are partially correlated with the ambient scattering. A tag or receiver that is not co-located with the radar would first need to sample the incident radar waveform. Mismatches in the sampled radar waveform could then result in communication waveforms generated at the tag that are different than the waveforms generated at the receiver.

Three situations that would cause changes in the sampled radar waveform are explored by examining the effect of those differences on the resulting communication waveforms. The first scenario considered is distortion of the incident radar waveform by forward scatter (i.e. multipath). A tag (or remote receiver) could receive multiple copies of the transmitted radar waveform due to reflections off objects being illuminated by the radar. The multiple copies received from the multipath channel can also cause the radar waveform to appear longer, making it difficult to determine the exact length of the transmitted waveform. The second mismatch situation explored is then when the tag and receiver determine different lengths for the sampled radar waveform used in the symbol generation, but without distortion. The last mismatch that is considered occurs from the tag and receiver using different sampling rates for the incident radar waveform.

The second practical aspect considered is when the receiver is not synchronized with the symbol waveform sent by the tag. The simulations to determine the probability of symbol error, performed previously in [1]-[4], assumed that the receiver had exact knowledge of the time delay of the embedded communication signal. The receiver could then use the filter output at the match point to determine the most likely symbol sent. If the time delay is not known, the receiver would need to search over multiple samples to extract the embedded symbol, increasing the probability of a symbol error.

Attempts will also be made to improve the waveform design with the goal of reducing errors and/or the probability of intercept. In order to improve performance,

the time length, as well as the bandwidth, of the radar waveform can be expanded as added dimensionality for communication waveform design. A rule-of-thumb is then developed for the trade-off between temporal and bandwidth expansion for a given symbol error rate. The second attempt at improving waveform design is to modify the Dominant-Projection approach to generate symbols that have less cross-correlation. This is achieved with two different methods. The first is giving a larger weight to the previously generated symbol waveforms in the projection matrix when generating new symbols and the second is combining the approach with the Gram-Schmitt procedure. The third attempt at improving performance is to equalize the correlation of the symbol waveforms with the interference by using the Hadamard transform. This is done to remove any symbol biases in the receiver caused by some symbols having a higher correlation with the interference than other symbols. The final method explored for improving the symbol waveform design to reduce symbol errors is accomplished by adjusting the size of the non-dominant space used when generating the symbols with Dominant-Projection. When the size of the non-dominant space is reduced, more of the dominant space will be projected away and the communication waveforms will be less correlated with the clutter interference. As a result, less symbol errors should occur. However, reducing the correlation of the communication waveforms with the interference would also make them less hidden thus increasing the probability of intercept by an unintended receiver.

1.2 ORGANIZATION OF THESIS

The remainder of thesis is organized into the following chapters. Chapter 2 covers some of the background on radar-embedded communication, specifically covering the previous work on intra-pulse coding. In chapter 3, situations that may cause mismatches in the communication waveforms used by the tag and receiver are explored. Receiver synchronization issues are examined in chapter 4 with two methods explored for reducing the effect of a lack of synchronization. Attempts to improve communication waveform design are discussed in chapter 5. Conclusions and future work to be performed are presented in chapter 6.

CHAPTER 2

BACKGROUND

The foundation for radar embedded communication beyond on-off signaling started in 1948 with Stockman's idea of using mechanically controlled corner reflectors to modulate the backscatter radiation [6]. More information could then be conveyed from the target back to the receiver by changing the reflector over multiple pulses. This idea was then expanded upon to develop more methods to use modulated reflectors as a means of communication. The majority of the methods developed for embedding communication signals in radar backscatter involved changing the modulation from pulse to pulse. In [7]-[11], a phase-shift sequence is applied to the reflections over multiple pulses. The phase-shifts can be imparted in a way that, to an unintended receiver that does not know the sequence, the phase modulation appears to be a Doppler signature. This approach allows the communication to be covert. These inter-pulse modulation techniques, though, often require on the order of hundreds of pulses for the symbol sequence. This results in a low data rate on the order of bits per coherent processing interval (CPI), which translates to a throughput of only a couple of bits per second (bps).

By operating on a intra-pulse basis, the incident radar waveform is remodulated into one of K different symbol waveforms. This allows transmission on the order of a few bits per pulse. Therefore, a radar having a pulse repetition

frequency (PRF) in the kHz range would have a communication rate on the order of kilobits per second (kbps). This greatly increases the amount of data that can be sent and if the communication waveforms are properly designed, can still have a low probability of intercept.

In [12], convolutional coding is used as an intra-pulse technique to remodulate the incident waveform. This modulation can achieve data rates up to 256 kbps, but the convolution coding uses the same mathematical structure as physical scattering. This process would initially appear to have a higher probability of intercept, since standard radar detection could most likely be used to intercept the embedded symbol waveforms. More work is needed to compare the convolution modulation with the design approaches discussed below.

The intra-pulse waveform design methods developed in [1]-[4], which are further explored and expanded in this thesis, utilize the spectrum of the radar signal outside its passband as a place to embed a communication signal. Expanding the bandwidth of the radar waveform provides a design space for the communication waveforms. The waveforms are designed to be similar to the ambient scattering of the radar making them harder to detect and more covert, but separable enough at the intended receiver to have a low probability of symbol error. The design of the communication waveforms is further discussed in the next section.

2.1 WAVEFORM DESIGN

As discussed above, the three intra-pulse waveform design approaches take advantage of the spectral bleeding of the radar signal for embedding covert communication signals. This spreading of the radar spectrum is shown below in figure 2.1.1. Since the radar occupies its entire passband, expanding into this bleeding region provides space to design the communication waveforms. In order for the communication waveforms to have a low probability of intercept (LPI), each of the three design methods generate waveforms that are partially correlated with the ambient scattering of the radar signal. This similarity allows the communication waveforms to be better hidden by the interference. The process of generating the symbol waveforms to be similar to the ambient scattering is further discussed below.

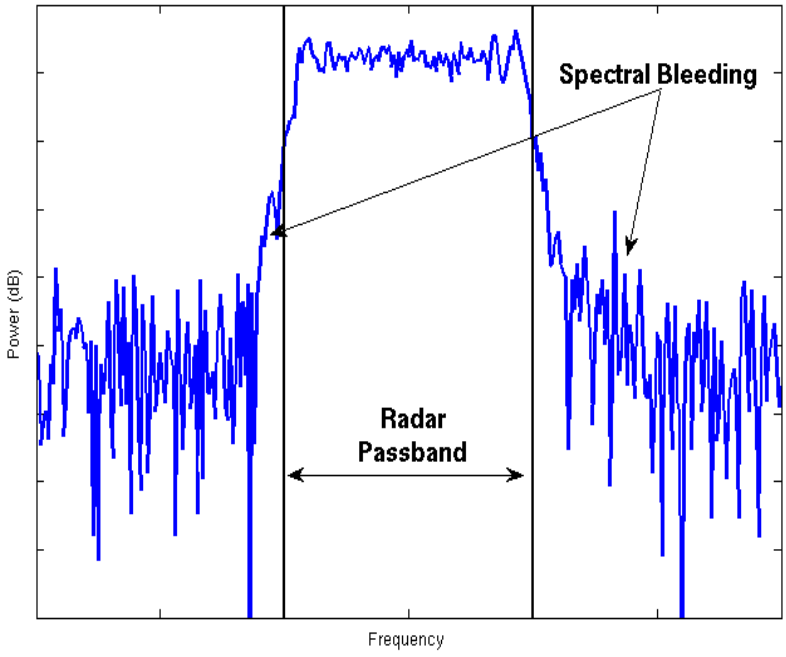

Figure 2.1.1: Radar spectral "bleeding" effect.

First, let $s(t)$ be the transmitted radar waveform. Oversampling this waveform by a factor of M results in the NM length vector $\mathbf{s}=[\mathrm{s}_0\ \mathrm{s}_1\ \ldots\ \mathrm{s}_{\mathrm{NM}-1}]^{\mathrm{T}}$, where N is the length of the radar waveform when sampled at Nyquist and $(\cdot)^T$ is the transpose operation. The ambient scattering of the radar waveform could then be modeled as

$$\mathbf{Sx}=\begin{bmatrix} s_{NM-1} & s_{NM-2} & \cdots & s_0 & 0 & \cdots & 0 \\ 0 & s_{NM-1} & \cdots & s_1 & s_0 & \cdots & 0 \\ \vdots & \vdots & \ddots & \vdots & \vdots & \ddots & \vdots \\ 0 & 0 & \cdots & s_{NM-1} & s_{NM-2} & \cdots & s_0 \end{bmatrix}\mathbf{x} \qquad (2.1)$$

where the $NM\times(2NM-1)$ matrix $\mathbf{S}$ is the the set of $2NM-1$ possible delay shifts of the sampled incident radar waveform $\mathbf{s}$ and the vector $\mathbf{x}$ is the range profile of the ambient scattering. A convenient basis for the generation of the communication waveforms is obtained from the eigen-decomposition of the correlation of $\mathbf{S}$ as

$$\mathbf{SS}^H=\mathbf{V}\boldsymbol{\Lambda}\mathbf{V}^H \qquad (2.2)$$

where $\mathbf{V}=[\mathbf{v}_0\ \mathbf{v}_1\ \ldots\ \mathbf{v}_{NM-1}]$ are the NM eigenvectors, $\boldsymbol{\Lambda}$ is a diagonal matrix of the associated eigenvalues (in order of decreasing magnitude) and $(\cdot)^H$ is the Hermitian operator. Figure 2.1.2 shows a plot of the eigenvalues of $\mathbf{SS}^H$ with a linear frequency modulated (LFM) waveform oversampled by a factor of $M=2$. In the plot, we see that the eigenvalues are roughly divided into dominant and non-dominant spaces, but there is a similar "bleeding" of values into the non-dominant space. The Eigenvectors-as-Waveforms, Weighted-Combining and Dominant-

Projection waveform design approaches utilize the non-dominant space for the communication waveforms. Each uses a different method of using the eigenvectors of $\mathbf{S}\mathbf{S}^H$ to generate the K symbols $\mathbf{c}_k$.

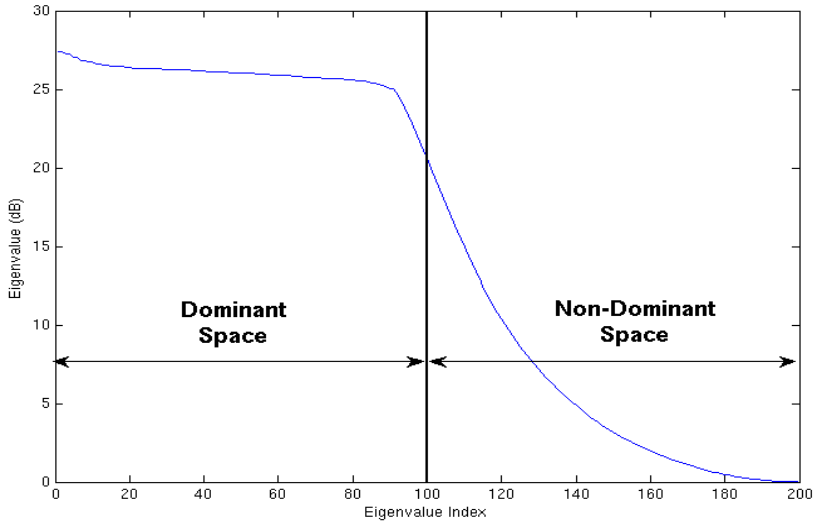

Figure 2.1.2: Eigenvalue plot with the radar waveform oversampled by 2.

2.1.1 EIGENVECTORS-AS-WAVEFORMS

The simplest design method uses a subset of the individual eigenvectors of the correlation matrix $\mathbf{S}\mathbf{S}^H$ for the communication waveforms. The least dominant eigenvectors are used such that each will have equal interference with the radar scattering. The communication waveforms are then the eigenvectors with the smallest eigenvalues as

$$\mathbf{c}_k = \mathbf{v}_{NM-k} \quad \text{for} \quad k = 1 \ldots K. \tag{2.3}$$

The resulting waveforms occupy a narrow bandwidth outside of the radar spectrum and have low correlation with the clutter interference. Due to this, the Eigenvectors-

as-Waveforms approach has the best performance in terms of symbol error rate, but it is also easy for an intercept receiver to detect and is the worst performer in terms of having a low probability of intercept (LPI).

2.1.2 WEIGHTED-COMBINING

The Weighted-Combining approach "spreads" the communication waveforms over the available design space. This spreading of the waveforms over the available non-dominant subspace is similar to spread spectrum communication [13], which spreads the power of the signal over a larger bandwidth than required for the given data rate. With spread spectrum signals, the power of the signal can even be dropped below the noise, making intercept by an unintended receiver difficult.

The spreading of the communication waveforms is accomplished by computing a weighted sum of the L individual, non-dominant eigenvectors. These non-dominant eigenvectors, given as

$$\mathbf{V}_{\mathrm{ND}} = [\,\mathbf{v}_{NM-L} \cdots \mathbf{v}_{NM}\,] \tag{2.4}$$

are a subset of $\mathbf{V}$ and are combined as

$$\mathbf{c}_k = \mathbf{V}_{\mathrm{ND}}\,\mathbf{b}_k \quad \text{for} \quad k = 1 \ldots K \tag{2.5}$$

to generate each communication waveform, where $\mathbf{b}_k$ is a Gaussian weight vector of length L known to both the tag and the receiver. The Weighted-Combining approach, by combining eigenvectors with larger eigenvalues, has more correlation with the ambient scattering. The waveforms are therefore less likely to be intercepted by an unintended receiver, but it also increases probability of symbol error.

2.1.3 DOMINANT-PROJECTION

Instead of directly using the non-dominant eigenvectors to generate the communication waveforms he Dominant-Projection approach a projects away from the eigenvectors corresponding to the dominant space resulting in waveforms spread across the entire non-dominant space. Since the dominant space is used as a whole, the approach is less susceptible to changes in the individual indexed eigenvectors used in the other two approaches. The Dominant-Projection design method also spreads the communication waveform over the design space resulting in a similar symbol error rate and probability of intercept as the Weighted-Combining approach.

In order for the communication waveforms to be separable at the receiver, they should be designed to be pairwise orthogonal. With the other two approaches, that use either the individual or combinations of the eigenvectors (which are each orthogonal), the resulting communication waveforms will be orthogonal. For Dominant-Projection, each new communication waveform needs to be projected away from any previously generated waveform as well as the eigenvectors of the dominant space. Therefore, when generating the k^{th} communication waveform, any previously generated waveform is appended to the scattering matrix $\mathbf{S}$ as

$$\mathbf{S}_k = [\mathbf{S}\ \mathbf{c}_1 \ldots \mathbf{c}_{k-1}] \quad . \tag{2.6}$$

The new eigen-decomposition is then

$$\mathbf{S}_k \mathbf{S}_k^H = \mathbf{V}_k \mathbf{\Lambda}_k \mathbf{V}_k^H \tag{2.7}$$

where $\mathbf{V}_k = [\mathbf{v}_{k,0}\ \mathbf{v}_{k,1} \ldots \mathbf{v}_{k,NM-1}]$ are the NM eigenvectors. The projection matrix

is generated by subtracting away the $NM+k-1-L$ eigenvectors corresponding to the dominant space as

$$\mathbf{P}_k = \mathbf{I} - \sum_{i=0}^{NM+k-L-2} \mathbf{v}_{k,i}\mathbf{v}_{k,i}^H \tag{2.8}$$

where $\mathbf{I}$ is an $NM \times NM$ identity matrix. The size of the dominant space that is included in the projection matrix is increased by $k-1$ to accommodate for the addition of the previously generated communication waveforms that are now present in the eigen-decomposition. Each communication waveform is generated as

$$\hat{\mathbf{c}}_k = \mathbf{P}_k \mathbf{b}_k \tag{2.9}$$

where $\mathbf{b}_k$ is a seed vector known to both the tag and receiver and then normalized as

$$\mathbf{c}_k = \frac{\hat{\mathbf{c}}_k}{\left\|\hat{\mathbf{c}}_k\right\|} \quad . \tag{2.10}$$

2.2 RECEIVER DESIGN

For radar-embedded communication, the similarity of the communication waveforms to the radar clutter that allows for hiding the signal for covert communication, can provide additional obstacles for the receiver design. Previous work on the receiver design performed in [1]-[4] is outlined below.

The NM length vector of the sampled received signal (assuming synchronization) is

$$\mathbf{r} = \mathbf{c}_k + \mathbf{S}\tilde{\mathbf{x}} + \mathbf{v} \tag{2.11}$$

where $\mathbf{c}_k$ is the communication symbol, $\tilde{\mathbf{x}}$ is a length $2NM-1$ vector of the radar range profile of the clutter (not necessarily the same as in equation 2.1) and $\mathbf{v}$ is NM samples of additive noise. Using a matched filter, the embedded communication symbol can be determined by selecting the symbol that satisfies

$$\hat{k} = \arg\left\{ \max_k \left(|\mathbf{c}_k^H \mathbf{r}| \right) \right\}. \tag{2.12}$$

Due to the relative power levels needed to hide the communication waveform in the backscatter of the radar and the correlation of the waveforms with the ambient scattering, the high interference levels cause significant degradation in symbol error rate performance when a matched filter is used.

Similar to a CDMA (code division multiple access) system which must separate out the symbol waveforms from the individual users using the same bandwidth, the receiver for radar embedded communication must separate the individual symbol waveforms as well as delayed copies of the radar waveform caused by the clutter interference. A variation of the decorrelating receiver in [14],[15] was then developed in [1]-[4] to improve the symbol error rate performance of the receiver. The $NM \times (2NM + K - 1)$ matrix

$$\mathbf{C} = [\mathbf{S}\ \mathbf{c}_1 \ldots \mathbf{c}_K] \tag{2.13}$$

is formed by appending the symbol waveforms $\boldsymbol{c}_k$ to the scattering matrix $\mathbf{S}$ and represents the possible interference and signal components that could be present in the received signal $\mathbf{r}$. The k^{th} decorrelating filter is then

$$\mathbf{w}_k = (\mathbf{C}\mathbf{C}^H)^{-1}\mathbf{c}_k \quad \text{for} \quad k = 1, 2, \ldots, K \tag{2.14}$$

and equation 2.11 is changed to select the embedded waveform as

$$\hat{k} = \arg\left\{ \max_k \left\{ \left| \mathbf{w}_k^H \mathbf{r} \right| \right\} \right\} \quad . \tag{2.15}$$

With its ability to better separate out the symbol waveform from the interference, the decorrelating filter achieves much better symbol error rate performance than when the matched filter is used.

CHAPTER 3

WAVEFORM MISMATCHES BETWEEN TAG AND RECEIVER

Chapter 2 presented the three previously developed design approaches for generating communication waveforms for intra-pulse radar embedded communication. In each approach, the incident radar waveform is used in the communication waveform generation process such that each symbol is sufficiently similar to the ambient scattering. This allows for the communication waveforms to remain hidden and to have a low probability of intercept (LPI), but separable enough to have a viable symbol error rate. Any mismatch between the radar waveform used by the tag and the radar waveform used by the receiver may result in the symbol waveforms being different, thereby increasing the probability of symbol error.

Each of the three design methods for the communication waveforms start with oversampling the incident radar waveform $s(t)$ by a factor of M. This results in the sampled radar waveform vector $\mathbf{s}=[s_0\ s_1 \ldots s_{NM-1}]^T$ of length NM, where N is the length of the radar waveform sampled at the Nyquist rate. The $NM\times(2NM-1)$ matrix

$$\mathbf{S}=\begin{bmatrix} s_{NM-1} & s_{NM-2} & \cdots & s_0 & 0 & \cdots & 0 \\ 0 & s_{NM-1} & \cdots & s_1 & s_0 & \cdots & 0 \\ \vdots & \vdots & \ddots & \vdots & \vdots & \ddots & \vdots \\ 0 & 0 & \cdots & s_{NM-1} & s_{NM-2} & \cdots & s_0 \end{bmatrix} \tag{3.1}$$

is then the set of $2NM-1$ possible delay shifts of the sampled incident radar

waveform $\mathbf{s}$. The three previously developed design approaches each have different methods of using the eigenvectors of $\mathbf{SS}^H$ to generate the K communication waveforms $\mathbf{c}_k$.

If the tag and receiver each have different versions of the sampled radar waveform vector $\mathbf{s}$, the eigenvectors of the correlation matrix $\mathbf{SS}^H$ used to produce the communication waveforms may also be different. Figure 3.1 shows a conceptual illustration of mismatches occurring in these eigenvectors with some eigenvectors moving to different indexes as well as mixed with other eigenvectors.

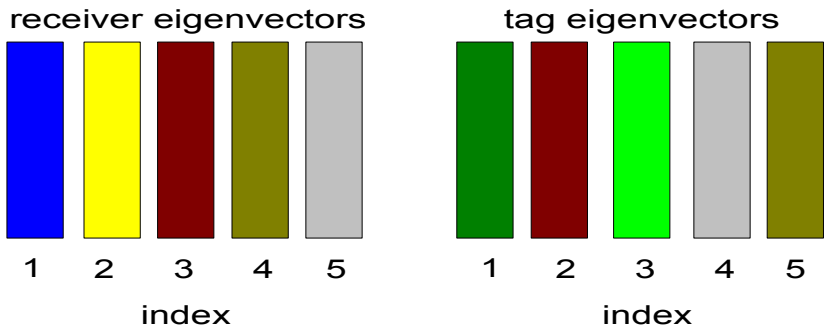

Figure 3.1: Illustration of eigenvector mismatches.

In this chapter, we will consider three situations where the radar waveform $s(t)$ that is incident at the tag and receiver may be different. In the first case, the the incident waveforms are different due to distortion caused by forward scattering effects (i.e. multipath). The second mismatch situation considered is if the tag and receiver use different lengths N to sample the incident radar waveform. We will also examine mismatches occurring due to the tag and receiver having different sampling rates, resulting in each having a different oversample value M.

3.1 FORWARD SCATTERING (MULTIPATH)

The radar signal incident at the tag (or a receiver not co-located with the radar) may include multiple copies of the waveform due to reflections off objects within the radar's illumination. An illustration of the multiple paths that the signal can travel between the transmitter and the tag causing multiple, delayed copies of the waveform being incident is shown in figure 3.1.1. In the radar literature, these reflections are generally known as forward scattering; in communications, they are known as multipath. In this section, we consider the situation in which the tag is located in a multipath environment and the receiver is the radar receiver and thus, has the exact waveform that is transmitted. Multipath distortion of the symbol waveforms from the tag to the receiver will not be considered in this chapter; it will be discussed later in section 4.5.

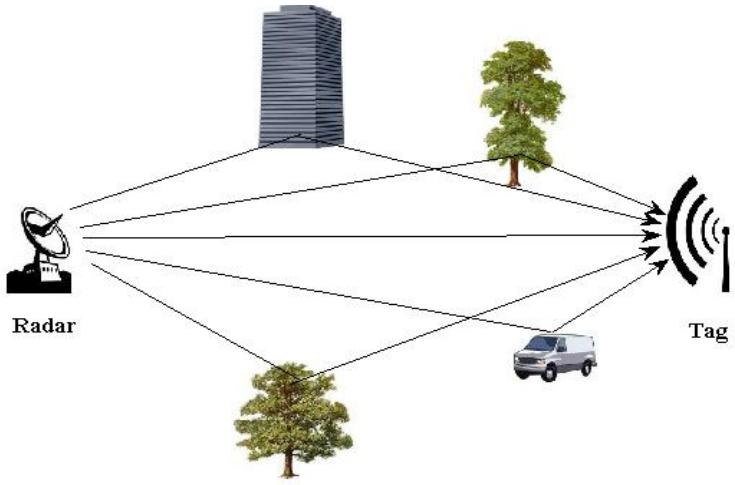

Figure 3.1.1: Illustration of multipath propagation.

To simulate the effect of the multipath environment on the radar waveform incident at the tag, the impulse response of the channel $h(t)$ is generated based on a multipath model. The distorted radar waveform $\tilde{s}(t)$ received at the tag is then

$$\tilde{s}(t) = s(t) * h(t) \tag{3.2}$$

where $*$ is the convolution operation. Three different multipath models are simulated: 1) an impulse at $t=0$ and additive white Gaussian noise, 2) the same impulse with a second, randomly delayed impulse having a random complex amplitude, and 3) a severe multipath scenario with many randomly delayed impulses each with a random complex value (including the direct path component).

For the simulations in this chapter, a sampled linear frequency modulated (LFM) radar waveform of type P3 from [16] is used with a length of $N=100$. In order to simulate the continuous nature of $s(t)$, the P3 radar waveform is oversampled by a factor of $M_c=10$ given as

$$s_c(n) = \mathrm{e}^{j\frac{\pi}{N}\left(\frac{n}{M_c}\right)^2} \tag{3.3}$$

for $n=[0\ 1\ \ldots\ NM_c-1]$, which results in the NM_c length vector $\mathbf{s}_c$. The oversampled version of the multipath distorted radar waveform is then

$$\tilde{\mathbf{s}}_c = \mathbf{s}_c * \mathbf{h} \tag{3.4}$$

where $\mathbf{h}$ is the sampled version of the channel impulse response and $*$ is the convolution operation. The tag truncates $\tilde{\mathbf{s}}_c$ to the correct length and samples the result to obtain $\tilde{\mathbf{s}}$ and the receiver samples the undistorted $\mathbf{s}_c$ to obtain $\mathbf{s}$, each

having a final oversampling rate of $M=2$ and length of $NM=200$. The tag and receiver use the vectors $\tilde{\mathbf{s}}$ and $\mathbf{s}$ to generate $K=4$ communication waveforms $\tilde{\mathbf{c}}_k$ and $\mathbf{c}_k$ respectively, using the three design approaches described in sections 2.1.1-3. The Weighed-Combining and Dominant-Projection approaches use $L=100$ for the size of the non-dominant space. The tag transmits the communication waveforms $\tilde{\mathbf{c}}_k$ generated from the multipath distorted radar waveform and the receiver uses the decorrelating filters $\mathbf{w}_k$ from $\mathbf{c}_k$ generated without multipath as in equation (2.14), to detect the transmitted waveforms via equation (2.15).

Monte Carlo simulations are run simulating 10,000 symbol transmissions with a new multipath profile independently generated every 100 symbols. For each of the simulations, a symbol to interference ratio (SIR) of -35 dB is used with the signal to noise ratio (SNR) varied from -15 dB to 0 dB in 5 dB steps. The symbol error rate performance is compared for each of the three design approaches for generating the communication waveforms and for each of the three multipath models.

3.1.1 IMPULSE AND AWGN

The first forward scattering model considered is an impulse with additive white Gaussian noise (AWGN). This model represents multipath distortion caused by small local clutter around the tag. This is modeled mathematically as

$$h(t)=\delta(t)+n(t) \tag{3.5}$$

where $\delta(t)$ is the Dirac delta function and $n(t)$ is AWGN of length τ_{max} with an average power of η_0. With this model, a copy of the radar waveform from the

direct path (delta function) plus many smaller, delayed copies from the convolved AWGN are incident and sampled by the tag.

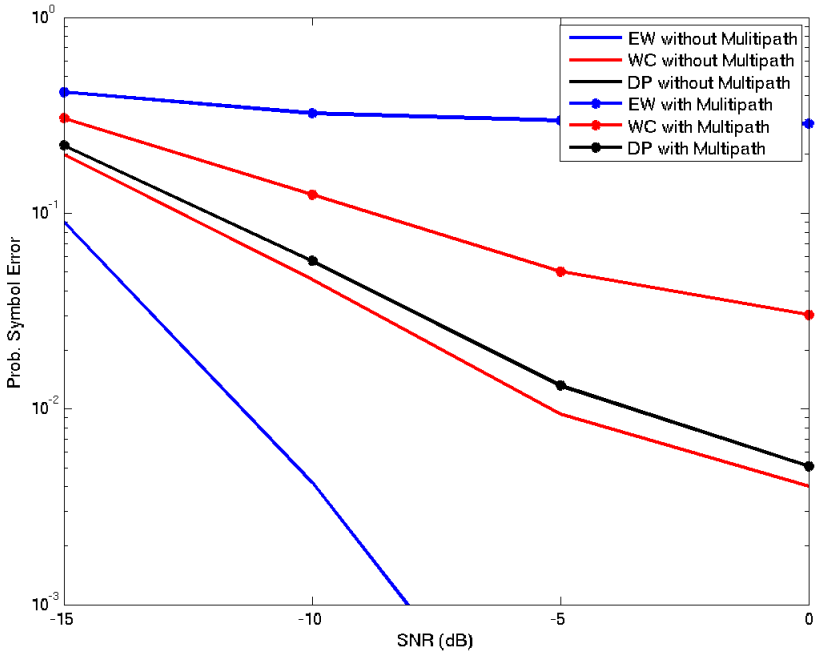

Figure 3.1.2: SER with and without impulse and -40dB AWGN multipath at the tag.

The symbol error rate (SER) results of the Monte Carlo simulation with $\tau_{max}=50$ samples of the radar waveform at Nyquist (i.e. 50% of the radar waveform length) and $\eta_0=-40\,dB$ are shown in figure 3.1.2. From the SER curves, we see that the Eigenvectors-as-Waveforms approach is most effected by the multipath distortion. Without multipath, it has the best SER performance, but with even this small amount of multipath it becomes the worst performer and is basically unusable. The Weighted-Combining approach is also affected by the multipath distortion, but the increase in the probability of symbol error is much less than with

the Eigenvectors-as-Waveforms approach. The SER performance with the communication waveforms generated by the Dominant-Projection approach appears to be completely unaffected by the multipath distortion at the tag.

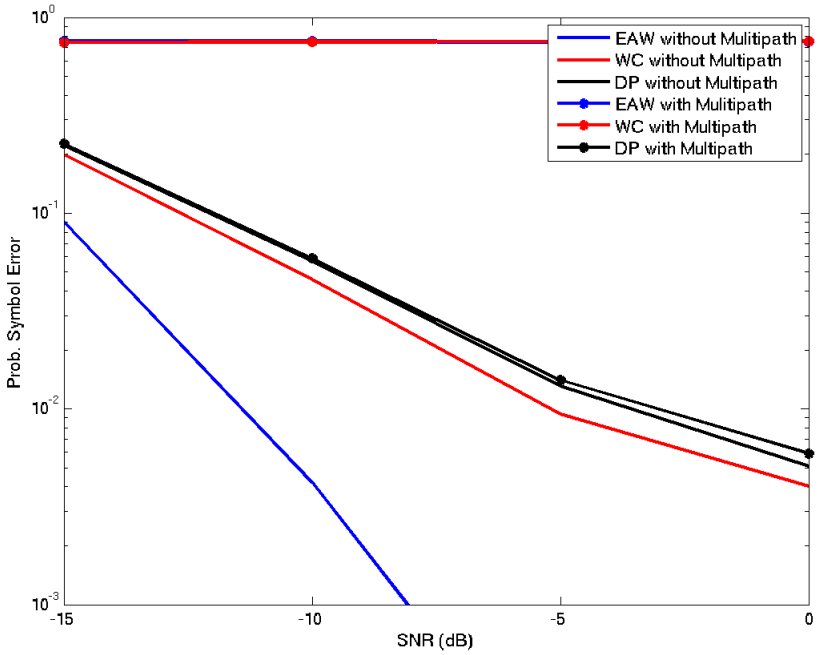

Figure 3.1.3: SER with and without impulse and -10dB AWGN multipath at the tag.

The simulation is again performed with $\tau_{max}=50$ samples, but with the power of the AWGN increased to $\eta_0=-10\,\mathrm{dB}$. The SER performance curves are shown in figure 3.1.3. In this scenario, both Eigenvectors-as-Waveforms and Weighted-Combining approaches break down and become unusable. With a probability of symbol error of about 0.75 and $K=4$ communication symbols, there appears to be enough of a mismatch in the communication waveforms that the receiver randomly selects which symbol was sent by the tag. The Dominant-

Projection approach, on the other hand, experiences only a negligible difference in the probability of symbol error, appearing virtually unaffected by the forward scatter seen by the tag.

3.1.2 IMPULSIVE CHANNEL

The next forward scattering model is th case when the tag receives a second, delayed copy of the radar waveform with magnitude commensurate with the direct path. This second copy of waveform could represent a reflection from another object such as a building, mountain or vehicle that is also illuminated by the radar. This single multipath component is larger on average than the multiple copies generated by the convolved AWGN in the previous. This multipath model is represented mathematically as

$$h(t)=\delta(t)+\rho\,\delta(t-\tau) \tag{3.6}$$

where $\delta(t)$ is the Dirac delta function, ρ is the complex Gaussian random amplitude of the reflector and τ is the time delay of the reflection uniformly distributed over $(0,\tau_{max}]$. The distorted radar waveform $\tilde{s}(t)$ received at the tag is then given by equation (3.2).

In figure 3.1.4, the probability of symbol error for each communication waveform design approach is compared with and without the multipath distortion from equation 3.6 and $\tau_{max}=50$ samples. The Eigenvectors-as-Waveforms and Weighted-Combining approaches both fail to produce usable communication waveforms when the tag experiences the multipath environment, as the probability of

symbol error of each is about 0.75. The Dominant-Projection approach, on the other hand, has no discernible degradation in SER performance from the added multipath component, again appearing robust to the distortion.

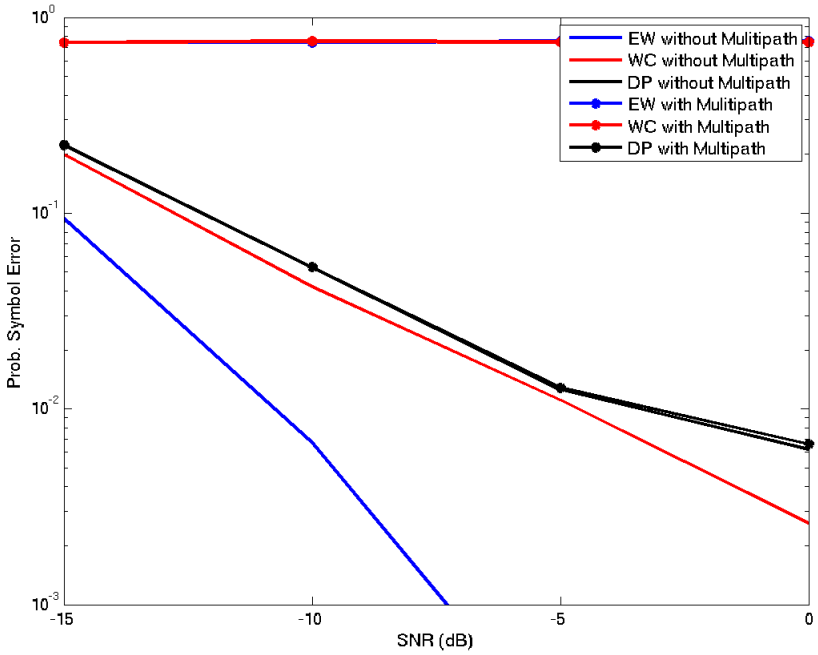

Figure 3.1.4: SER with and without multipath from a random impulse at the tag.

3.1.3 MANY RANDOM IMPULSES (SEVERE MULTIPATH)

The final forward scattering model considered is a severe multipath scenario with the tag receiving many random copies of the radar waveform. In this case, the direct path component at $t=0$ is not necessarily the most dominant copy received. For this scenario, the channel response is generated as

$$h(t)=\rho_0\delta(t)+\sum_{l=1}^{L-1}\rho_l\delta(t-\tau_l) \qquad (3.7)$$

where ρ_0 and ρ_l for $l=1,\ldots,L$ are i.i.d. complex Gaussian random variables, τ_l for $l=1,\ldots,L$ is uniformly distributed over $(0,\tau_{max}]$, and $\delta(t)$ is the Dirac delta function.

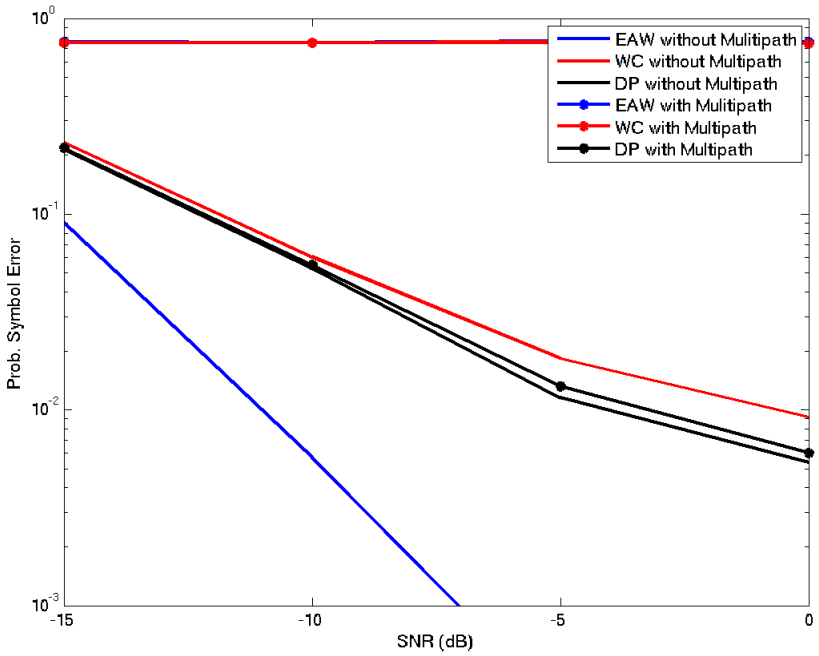

Figure 3.1.5: SER with and without the tag experiencing severe multipath.

The SER curves for the severe multipath simulation with $\tau_{max}=50$ samples are shown in figure 3.1.5. Consistent with the previous results, both the Eigenvectors-as-Waveforms and Weighted-Combining approaches break down and are unusable with the multipath distortion, while the Dominant-Projection approach, even in this severe multipath environment, generates communication waveforms with no discernible difference in symbol error rate performance compared to those generated without the multipath distorted radar waveform. The Dominant-Projection approach, therefore, appears to be robust to the effects of multipath distortion of the radar

waveform incident on the tag. The basis for Dominant-Projection as more robust waveform generation approach is further explored in the next section.

3.1.4 ROBUSTNESS OF DOMINANT-PROJECTION

In each of the multipath scenarios in sections 3.1.1-3 above, the SER performance of communication waveforms generated with both the Eigenvectors-as-Waveforms and Weighted-Combining approaches were severely degraded by moderate multipath distortion, but the Dominant-Projection approach remained mostly unaffected, even under severe multipath conditions. To determine the reason the dominant-projection approach is robust to the multipath distortion, we must look closer at the process for generating the communication waveforms.

Recall that in order to produce communication waveforms that are similar to the ambient scattering in an effort to remain LPI, each design method starts by generating the scattering matrix $\mathbf{S}$ representing the possible delay shifts of the sampled radar waveform $\mathbf{s}$. The ambient scattering would then be $\mathbf{Sx}$, where $\mathbf{x}$ is the range profile vector for the local clutter. In continuous time, the ambient local scattering is represented as the convolution

$$y(t)=s(t)*x(t) \tag{3.8}$$

where $x(t)$ is the impulse response of the illuminated radar range profile. This is observed to be the same operation governing the multipath distor in section 3.2 where the radar waveform $s(t)$ is distorted by the multipath channel $h(t)$ such that $\tilde{s}(t)=s(t)*h(t)$ is incident. Therefore, for the combination of multipath distortion

and ambient scattering, we can substitute (3.2) into (3.8), to obtain

$$y(t)=\tilde{s}(t)*x(t)=s(t)*h(t)*x(t)=s(t)*\acute{x}(t) \qquad (3.9)$$

where $\acute{x}(t)=x(t)*h(t)$ can just be treated as a different range profile. Multipath distortion thus has the same mathematical structure as the local scattering mimicked in the generation of the communication waveforms.

Each waveform design approach has a different method of utilizing the eigenvectors of the correlation matrix $\mathbf{S}\mathbf{S}^H$ to form the K communication waveforms $\mathbf{c}_k$. Although the multipath possesses the same mathematical structure as the ambient scattering modeled in $\mathbf{S}$, the distortion causes changes in the eigenvectors of $\mathbf{S}\mathbf{S}^H$. Depending on the design approach, the eigenvector mismatches can cause the generation of different communication waveforms. To understand the differences in the eigenvectors caused by the multipath distortion, we will look at the correlation between the sets of eigenvectors with and without the multipath distortion to compare their similarities and differences.

From section 2.1, the matrix $\mathbf{V}$ is the set of eigenvectors of the correlation matrix $\mathbf{S}\mathbf{S}^H$ used to generate the communication waveforms. Let the matrix $\tilde{\mathbf{V}}$ be the set of eigenvectors from $\tilde{\mathbf{S}}\tilde{\mathbf{S}}^H$, where $\tilde{\mathbf{S}}$ is obtained via (3.1) using the vector $\tilde{\mathbf{s}}$, the sampled version of the multipath distorted radar waveform $\tilde{s}(t)$. The correlation of the two sets of eigenvectors is then calculated as $|\tilde{\mathbf{V}}^H\mathbf{V}|$. If the eigenvector sets are identical (i.e $\mathbf{V}=\tilde{\mathbf{V}}$), the resulting correlation would be $|\tilde{\mathbf{V}}^H\mathbf{V}|=|\mathbf{V}^H\mathbf{V}|=\mathbf{I}$ where $\mathbf{I}$ is the identity matrix.

As in sections 3.1.1-3, a P3 radar waveform of length $N=100$ is used and oversampled by a factor of $M=2$. This results in the set of $MN=200$ eigenvectors. From the length and bandwidth of radar waveform, the eigenvectors with indices from 1 to 100 correspond to the dominant space occupied by the radar waveform with the non-dominant space consisting of the eigenvectors with indices from 101 to 200. The average eigenvector correlation $|\tilde{\mathbf{V}}^H \mathbf{V}|$ is calculated over 100 Monte Carlo simulations of different random multipath profiles to see how the distortion affects the eigenvector sets. Also, the correlation of the communication waveforms generated from each eigenvector set is averaged over the 100 multipath profiles to see the resulting effect of the changed eigenvectors for each of the three symbol waveform generation approaches. These results are then compared with the probability of symbol error results in sections 3.1-3.

The average eigenvector correlation is calculated for the impulse and AWGN multipath model in section 3.1.1 with random multipath profiles generated from equation (3.3) with $\eta_0 = -40\,\text{dB}$ and $\tau_{max}=50$ samples. The intensity plot of the eigenvector set correlation is shown in figure 3.1.6. From this simulation, we observe a smeared diagonal line of high correlation where the index of $\mathbf{V}$ is equal to the index of $\tilde{\mathbf{V}}$. If the two sets of eigenvectors were identical and $|\tilde{\mathbf{V}}^H \mathbf{V}| = \mathbf{I}$, the intensity plot would consist of a line at 0 dB on the diagonal and -∞ dB elsewhere. In this case, the multipath distortion appears to smear the eigenvectors, resulting in correlations occurring off of the diagonal. Here, signal components that exist in an

eigenvector at one index in $\mathbf{V}$ may be present in eigenvectors at other indexes within $\tilde{\mathbf{V}}$.

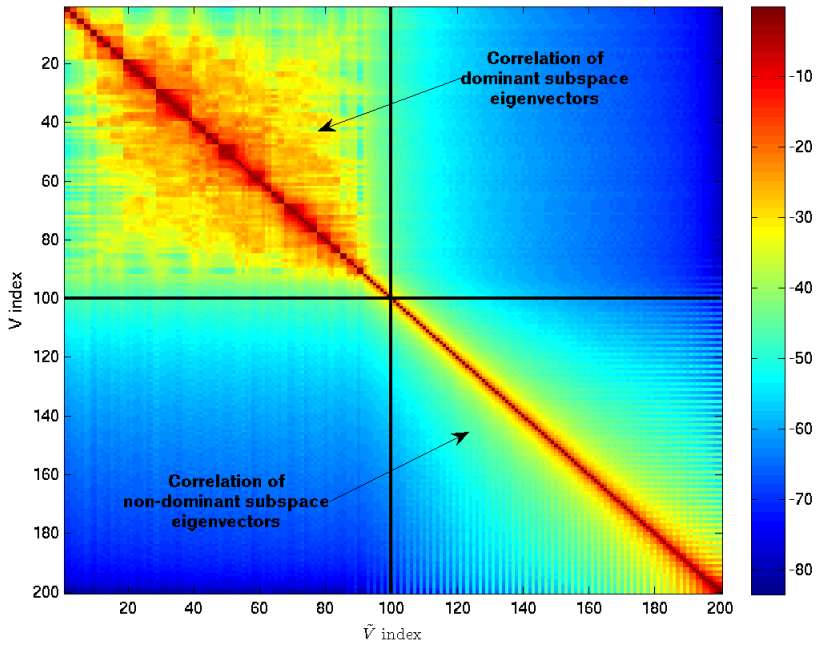

Figure 3.1.6: Eigenvector correlation intensity plot (in dB) with impulse and -40dB AWGN.

The average correlation of the communication waveforms produced at the receiver without multipath and the waveforms generated at the tag under this multipath condition are shown in figure 3.1.7. Here, the correlation for each of the four communication waveforms is averaged over the 100 random multipath profiles and shown for each of the three design approaches. Looking at the average correlations, each of the three methods continue to produce waveforms that are significantly correlated at the match point with the tag in the multipath environment. The waveforms generated by the Eigenvectors-as-Waveforms and Weighted-

Combining approaches, though, are slightly below 0 dB at 0 delay offset and therefore, are no longer perfectly matched. Also noted is that due to the narrow bandwidth of the communication waveforms produced with the Eigenvectors as waveforms approach, the correlation of the waveforms has a slower roll-off than the waveforms from the other two methods that are more spread out in bandwidth.

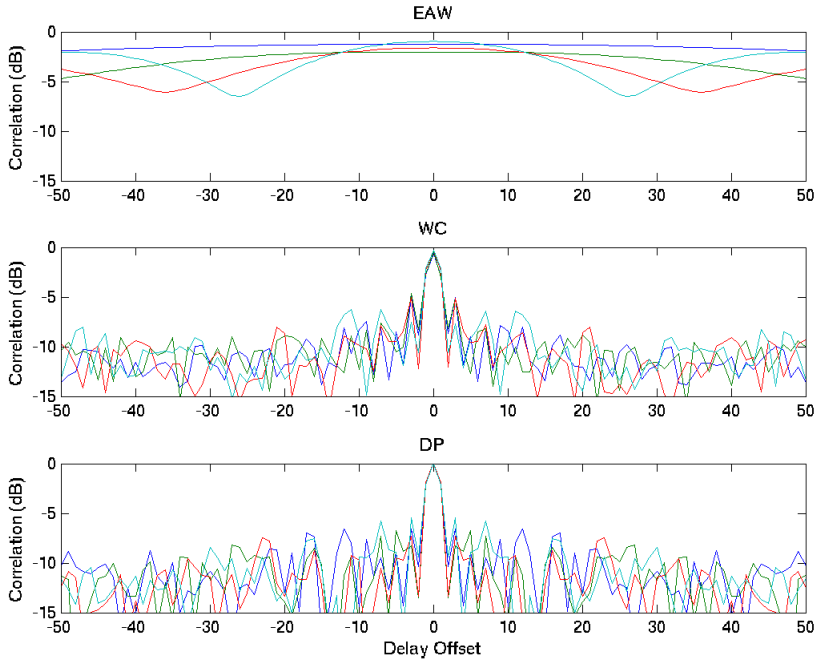

Figure 3.1.7: Symbol Correlations for impulse and -40 dB AWGN multipath.

The SER performance for this multipath scenario, as seen in figure 3.1.2, shows that the Eigenvectors-as-Waveforms approach suffered the most degradation from the multipath distortion. Recall that this approach uses the individual, least dominant eigenvectors for the communication waveforms. These are the eigenvectors with indexes near 200, which from figure 3.1.6 show smearing in their correlation.

This leads to the mismatch in the communication waveforms seen in figure 3.1.7 and degradation in SER performance. The Weighted-Combining approach, on the other hand, uses randomly weighted combinations of the L individual non-dominant eigenvectors. This approach also suffers degradation of SER performance under this multipath condition, but not to the degree that the Eigenvectors-as-Waveforms approach. Therefore, there must be a higher correlation of the combination of the eigenvectors of the non-dominant space than the individual least-dominant eigenvectors used in the Eigenvectors-as-Waveforms approach. Looking at figure 3.1.6, we see that the eigenvectors nearer to the dominant space (near index 100), appear to experience less smearing than the least dominant eigenvectors (near index 200). By combining these more correlated eigenvectors, the resulting communication waveforms are more correlated than the individual, least dominant eigenvectors.

If the power level of the noise is increased from $\eta_0 = -40\,\mathrm{dB}$ to $\eta_0 = -10\,\mathrm{dB}$ for the impulse and AWGN multipath model, we have the average correlation intensity plot shown in figure 3.1.8. For this situation, we observe that the smearing of the eigenvectors caused by the multipath distortion increases to the point that there is no longer a defined diagonal of high correlation where the index of $\mathbf{V}$ is equal to the index of $\tilde{\mathbf{V}}$.

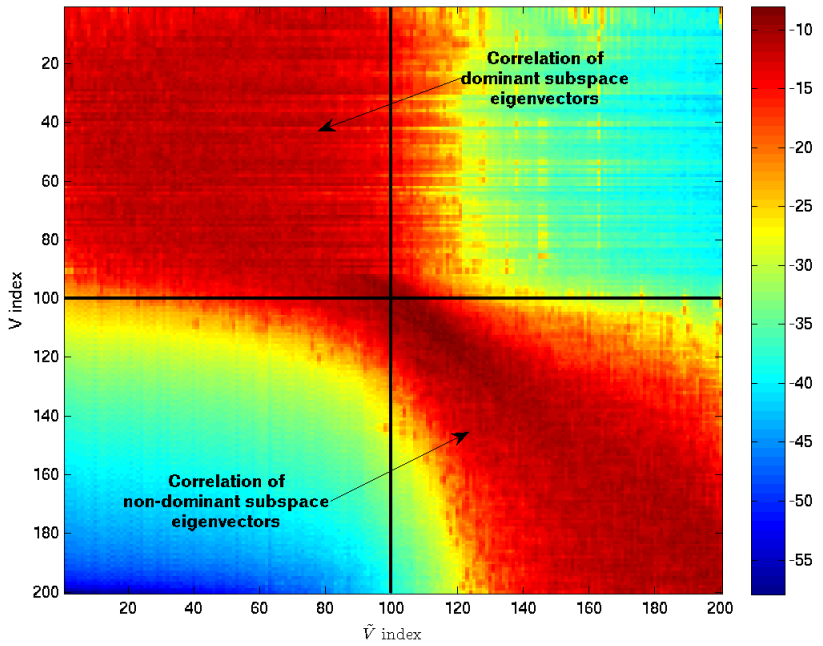

Figure 3.1.8: Eigenvector correlation intensity plot (in dB) with impulse and -10dB AWGN.

From the average correlation of the communication waveforms in figure 3.1.9, it is observed that the Eigenvectors-as-Waveforms and Weighted-Combining approaches now fail to produce matching communication waveforms with the receiver using the exact radar waveform and the tag using the multipath distorted waveform. The increased multipath distortion caused by the larger noise power smears the eigenvectors such that the indexed sets are no longer correlated. The Dominant-Projection approach, however, continues to generate communication waveforms that are highly correlated between the tag and receiver, with the correlation at the match point remaining near 0 dB.

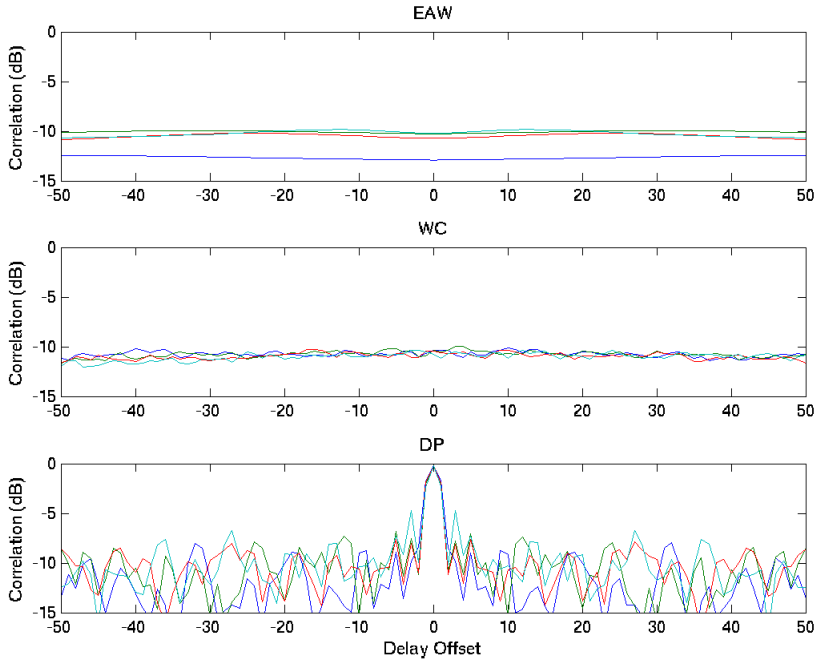

Figure 3.1.9: Symbol Correlations with impulse and -10 dB AWGN multipath.

The SER curves from figure 3.1.3 confirm the symbol waveform correlation results shown in figure 3.1.9. Both the Eigenvectors-as-Waveforms and Weighted-Combining approaches fail, as the symbol error performance is no better than that of random symbol selection. Since the eigenvectors are no longer correlated between the tag and receiver, both approaches, which use the indexing of the individual eigenvectors, generate communication waveforms that are uncorrelated between the tag and receiver with this multipath scenario. The Dominant-Projection approach remains unaffected and robust to the distortion.

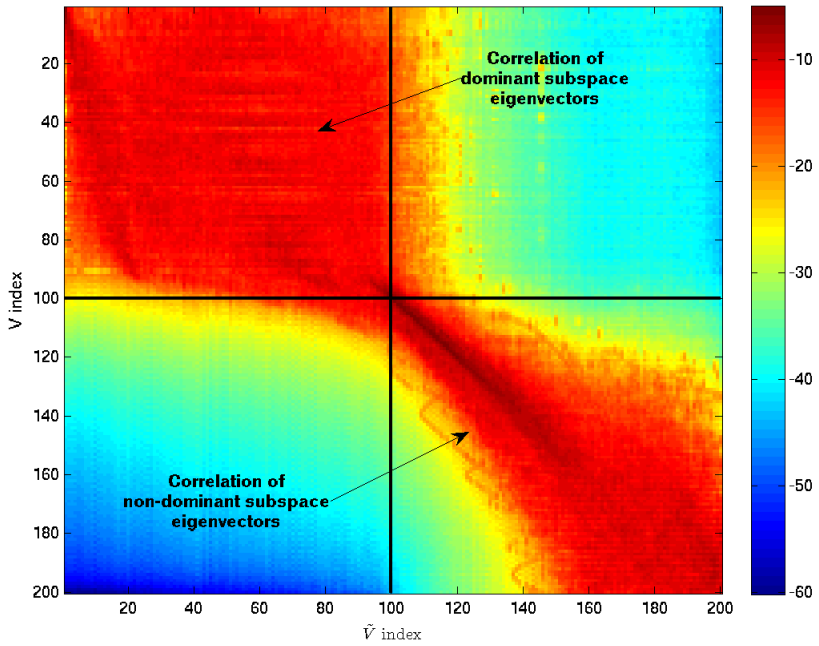

Figure 3.1.10: Eigenvector correlation intensity plot (in dB) with multipath from second random impulse seen by the tag.

Figure 3.1.10 shows the intensity plot of the average eigenvector correlation when the radar waveform experiences a second, randomly delayed, multipath component with a random complex amplitude with the model given equation (3.6). As was seen in figure 3.1.8 with an impulse and -10 dB of AWGN, there is again significant smearing of the eigenvectors off of the diagonal of equal indexes. This is caused by the second radar waveform component from the multipath reflection.

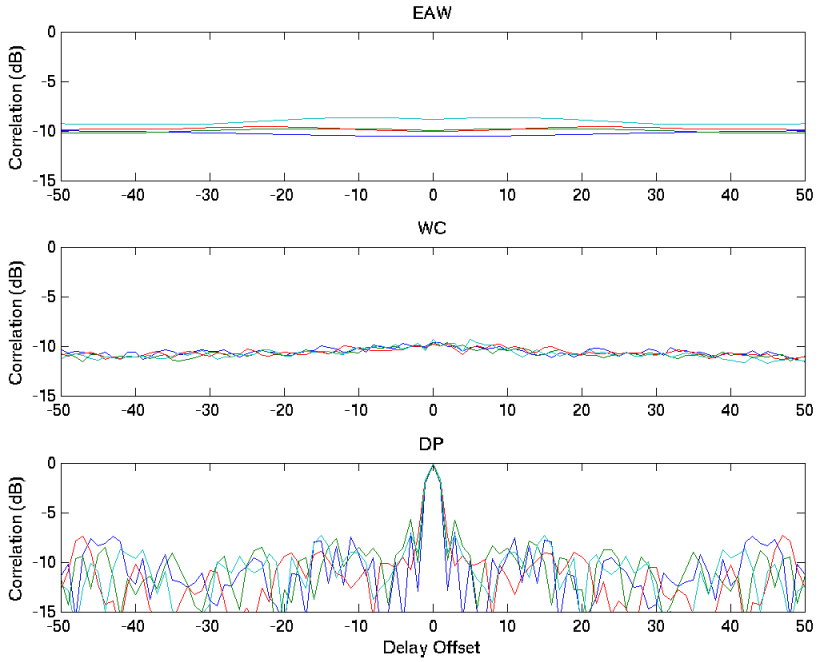

Figure 3.1.11: Symbol Correlations for multipath from second random impulse multipath.

The average communication waveform correlation for this multipath scenario is shown in figure 3.1.11. Again, both the Eigenvectors-as-Waveforms and Weighted-Combining methods do not produce communication waveforms that are similar enough to be effective, but the Dominant-Projection method still generates communication waveforms that are matched between the tag and receiver. This confirms the SER performance for this multipath model in figure 3.1.3, where the Eigenvectors-as-Waveforms and Weighted-Combining approaches fail and the Dominant-Projection approach is unaffected by the multipath distortion.

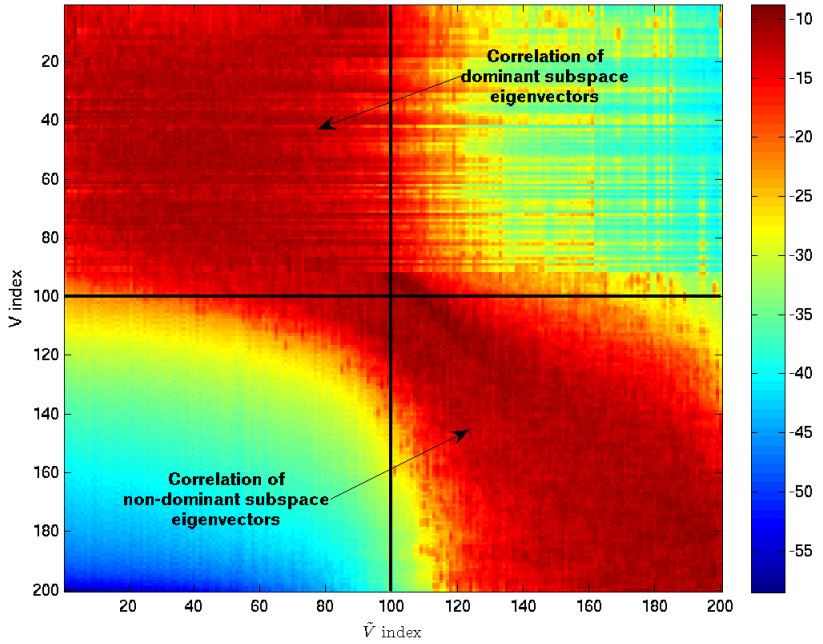

Figure 3.1.12: Eigenvector correlation intensity plot (in dB) with severe multipath at the tag.

For the severe multipath scenario given in equation (3.7), we have the average eigenvector correlation given by the intensity plot in figure 3.1.12. Again, we see a large amount of smearing of the eigenvectors caused by the multipath distortion. Unsurprisingly, the Eigenvector-as-Waveforms and Weighted-Combining approaches fail to produce communication waveforms at the tag that are correlated to the receiver waveforms when using the Eigenvectors-as-Waveforms and Weighted-Combining approaches, but even under this severe multipath distortion, the Dominant-Projection approach still produces matched waveforms. This is shown in the average symbol correlation in figure 3.1.13 and confirmed by the SER curves in figure 3.1.5.

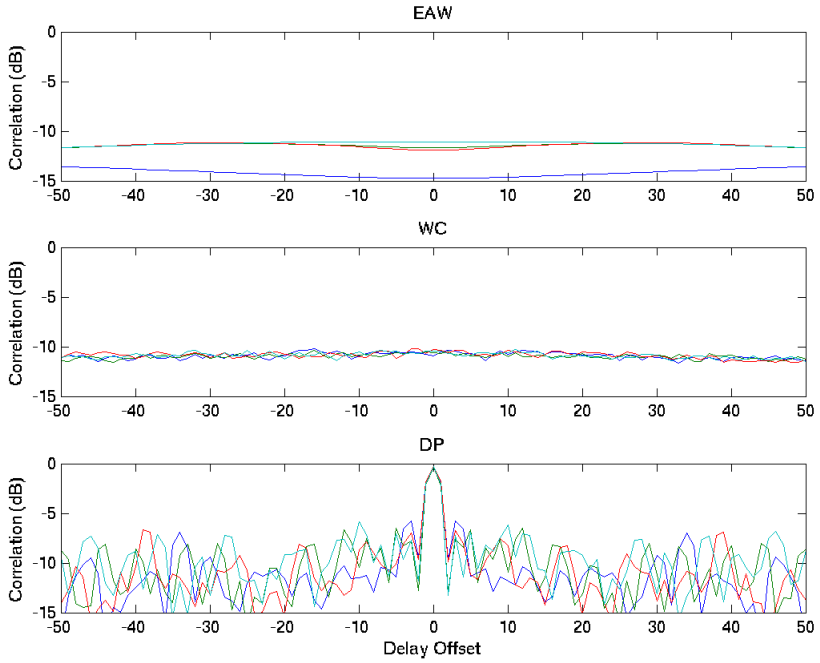

Figure 3.1.13: Symbol Correlations for multipath with severe multipath.

From the eigenvector correlation intensity plots above, we are able to directly see the smearing of the eigenvectors that cause the Eigenvectors-as-Waveform and Weighted-Combining approaches to fail. However, there is also a consistent aspect to each that leads to the reasoning the Dominant-Projection approach is robust to each of the models for multipath distortion. Instead of using the individual eigenvectors, the Dominant-Projection approach uses the set of eigenvectors corresponding to the dominant space as a whole to generate the communication waveforms. In each of the multipath scenarios, even with the severe case, while there is significant smearing of the individual eigenvectors, the dominant and non-dominant spaces remain mostly separate. This can be observed with the aid of the black lines in each of the intensity plots showing the division between the two subspaces. In the Dominant-Projection

procedure, when generating each new waveform, the eigenvectors of the dominant space and any previously generated communication waveform is projected away from a random vector that is known to both the tag and receiver. Although the individual eigenvectors at the tag are not the same, as seen in figures 3.1.5-8, most of the information is contained by each set of the dominant eigenvectors as a whole. This results in a similar projection away from the seed vector and matching communication waveforms are generated.

3.2 WAVEFORM LENGTH DIFFERENCES

Another problem caused by forward scatter is that the multiple, delayed copies of the radar waveform expand the apparent length of the received pulse. This can make it difficult to determine the exact length N to use for the incident radar waveform $\tilde{s}(t)$. This could, in turn, lead to mismatches in the generated communication waveforms used by the tag and receiver. An illustration of the time expansion of the radar signal is shown in figure 3.2.1. Here, the radar waveform is distorted by multipath as in section 3.1.1 with $\tau_{max}=50$ samples and $\eta_0=-10\,\text{dB}$. The multipath distorted waveform appears to continue well past the original waveform, making it appear longer. As a result, the tag and receiver could determine different lengths for the radar pulse and the generation of the communication waveforms that are no longer correlated.

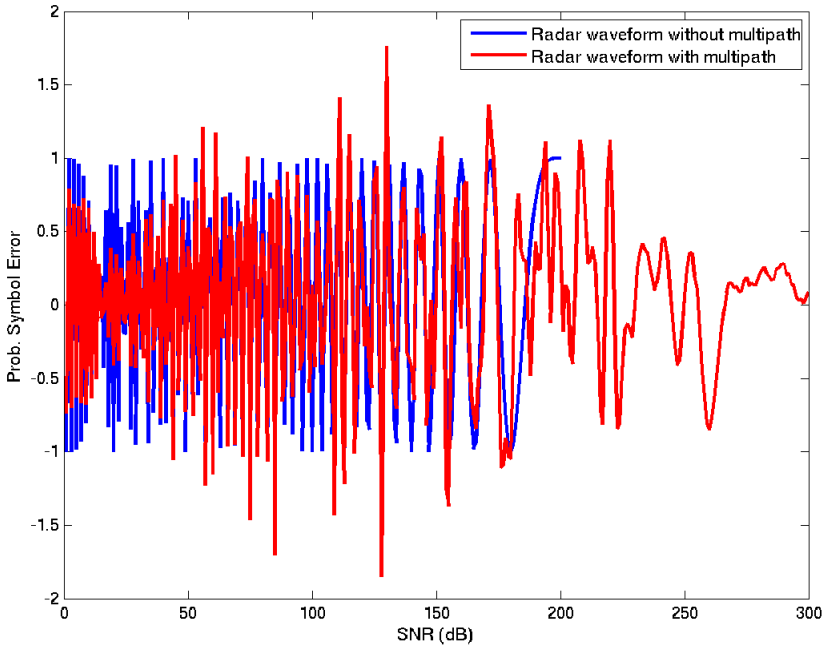

Figure 3.2.1: Radar waveform length ambiguity due to multipath.

In the previous simulations, both the tag and receiver were presumed to have exact knowledge of the radar waveform length N to be used in the generation of the communication waveforms. If either the tag or receiver (not in the radar) does not have prior knowledge of the length of the radar waveform, it would need to be determined from the incident waveform. As discussed above, this could lead it to use a different value for the length $\tilde{N}$ for the radar waveform. Here the undistorted radar waveform $s(t)$ is sampled to form the length $\tilde{N}M$ vector $\tilde{\mathbf{s}}$ used to generate the $\tilde{N}M \times (2\tilde{N}M - 1)$ scattering matrix $\tilde{\boldsymbol{S}}$. The set of eigenvectors $\tilde{\mathbf{V}}$ from $\tilde{\mathbf{S}}\tilde{\mathbf{S}}^H$ would then be used to generate the communication waveforms $\tilde{\mathbf{c}}_k$. For Weighted-Combining and Dominant-Projection the size of the non-dominant space would then be $\tilde{L} = (M-1)\tilde{N}$.

To simulate these waveform length differences between the tag and receiver, we will again use the P3 radar waveform with a length of $N=100$ and an oversample factor of $M=2$ to generate $K=4$ communication waveforms. The receiver is presumed to have the exact knowledge of the radar waveform length, but the length of the waveform used at the tag is varied from $\tilde{N}=50$ to $\tilde{N}=150$. Monte Carlo simulations are run simulating 10,000 symbol transmissions for each value of $\tilde{N}$. The symbol error rate is calculated for each of the three communication waveform design approaches and plotted in the figures below.

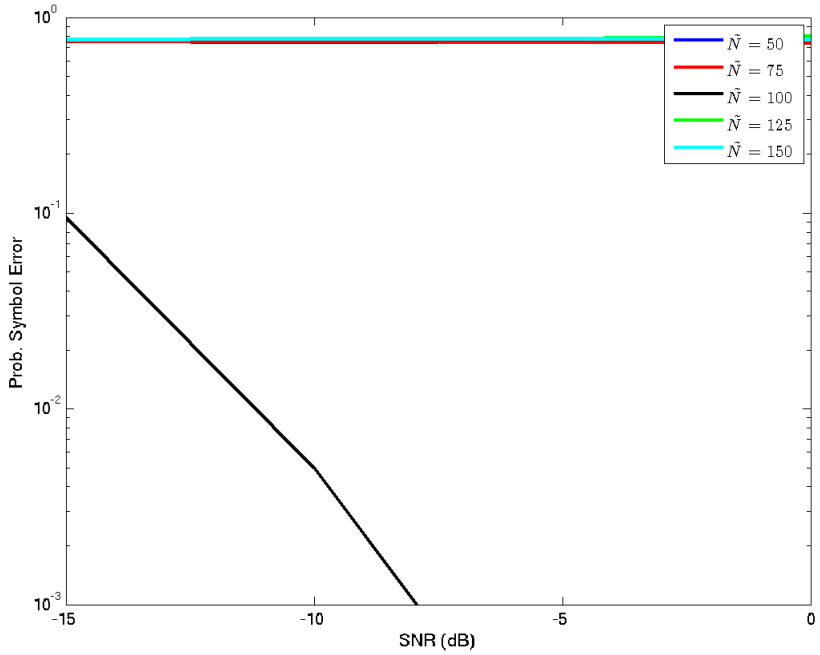

Figure 3.2.2: SER curves for length differences with Eigenvectors-as-Waveforms.

The symbol error rate curves for the Eigenvectors-as-Waveforms approach are shown in figure 3.2.2. Here we see that any value of $\tilde{N}$ used by the tag that is not

equal to the actual radar waveform length $N=100$ used by the receiver, results in an unusable symbol error rate, with the probability of symbol error at about 0.75. From the SER curves for the Weighted-Combining approach in figure 3.2.2 below, we observe that again any mismatch between $\tilde{N}$ and N renders it unusable. From the observations of section 3.1.4, it is suspected that a difference between $\tilde{N}$ and N will cause mismatches in the eigenvectors sets $\mathbf{V}$ and $\tilde{\mathbf{V}}$. The generated symbol waveforms from the different eigenvectors sets will be uncorrelated and unusable for communication.

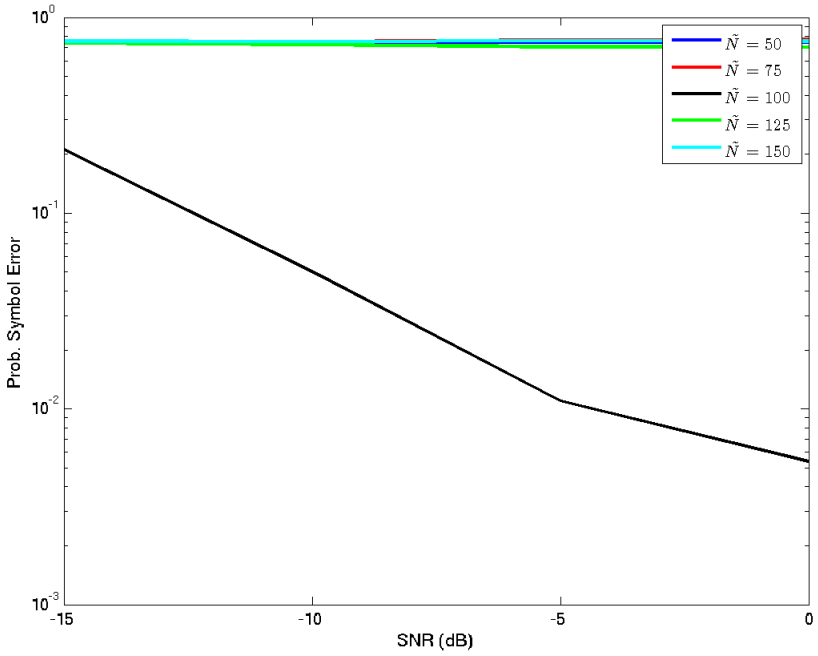

Figure 3.2.3: SER curves for length differences with Weighted Combining.

The SER curves for the different values of $\tilde{N}$ when the Dominant-Projection approach is used are shown in figure 3.2.4. From the plot, we see that when the tag uses a shorter radar waveform length of $\tilde{N}=75$, the SER performance at 0 dB SNR

is significantly degraded to about 0.08 from about 0.003 with the correct length of $\tilde{N}=100$. The probability of error gets even worse to about 0.4 when length of the radar waveform used at the tag is reduced to $\tilde{N}=50$. However, if the tag uses a longer radar waveform length of $\tilde{N}=125$ or $\tilde{N}=150$ the symbol error rate is mostly unchanged from when the correct length of the radar waveform is used. It then appears that the Dominant-Projection approach is also robust to differences in the radar waveform length, as long as the tag uses a length of the radar waveform that is equal or greater than the length used at the receiver. To gain a further understanding of why using a longer radar waveform at the tag does not affect the SER performance, we again will look at the correlations of the eigenvector sets when different waveform lengths are used.

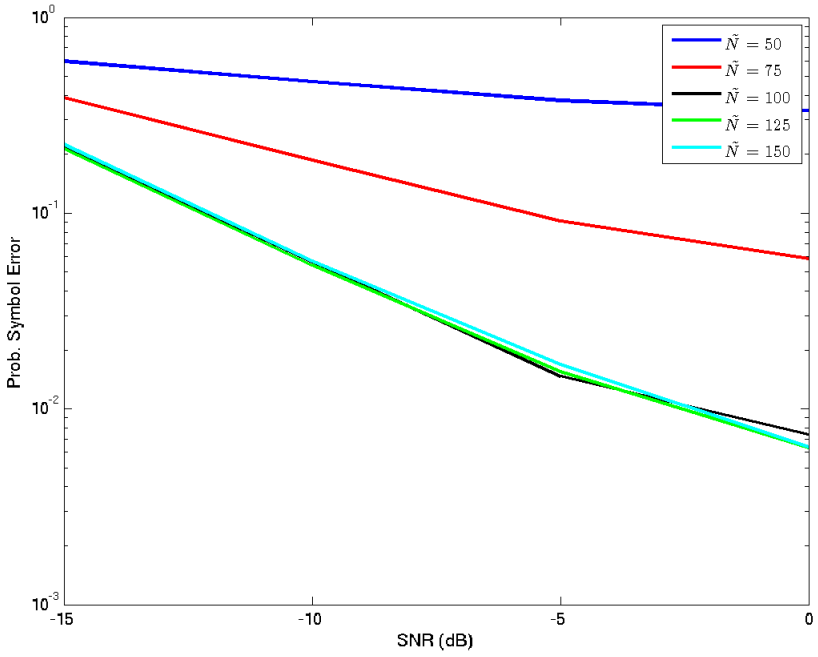

Figure 3.2.4: SER curves for length differences with Dominant-Projection.

To compare the eigenvector sets used by the receiver and tag in the communication waveform generation process, we will again calculate the correlation matrix $|\tilde{\mathbf{V}}^H \mathbf{V}|$. When $\tilde{N} \neq N$, the length of the eigenvectors in $\mathbf{V}$ will be different than those in $\tilde{\mathbf{V}}$. The shorter of the two is zero padded for the dimensionality to match to be able to calculate $|\tilde{\mathbf{V}}^H \mathbf{V}|$.

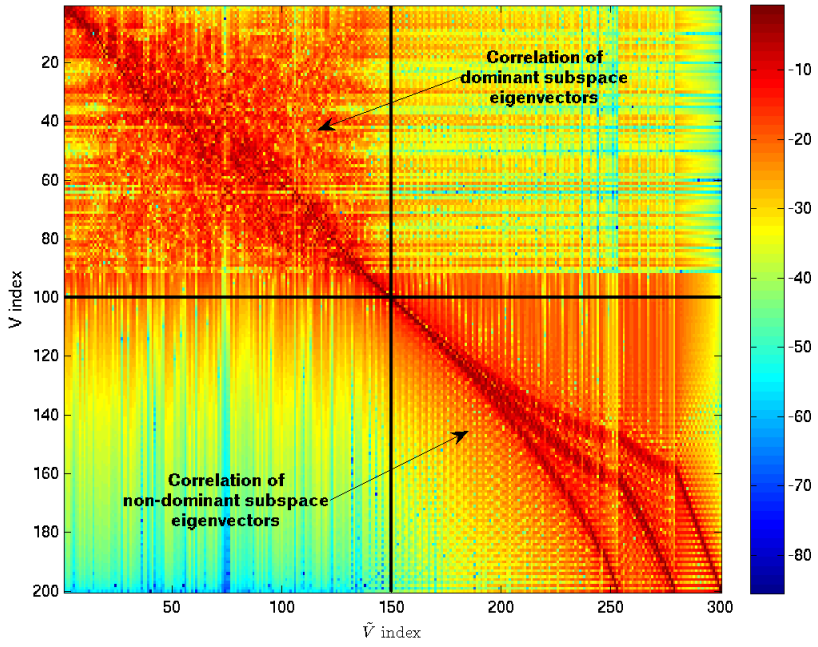

Figure 3.2.5: Eigenvector Correlation (in dB) with $N = 100$ *and* $\tilde{N} = 150$.

The eigenvector correlation intensity plot for the tag using a radar waveform length of $\tilde{N} = 150$ is shown in figure 3.2.5. From this plot, we again see the eigenvector smearing that is detrimental to the Eigenvectors-as-Waveforms and Weighted-Combining approaches. It can also be observed, that with the tag using a longer radar waveform, the dominant and non-dominant spaces remain mostly

separate. Here, the eigenvectors indexed between 1-100 and 101-200 in $\mathbf{V}$ are correlated mostly with eigenvectors of $\tilde{\mathbf{V}}$ indexed between 1-150 and 151-300 respectively.

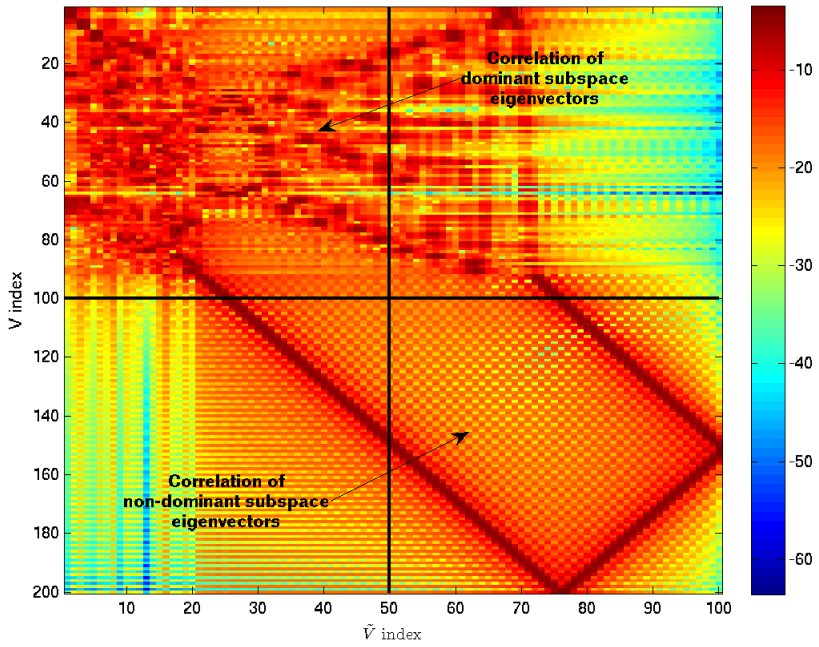

Figure 3.2.6: Eigenvector Correlation (in dB) with $N=100$ *and* $\tilde{N}=50$.

The eigenvector correlation when the tag uses a radar waveform length of $\tilde{N}=50$ is shown in figure 3.2.6. Here, the size of the non-dominant space that the tag estimates is $\tilde{L}=50$. From the intensity plot, we see that the dominant and non-dominant spaces no longer appear separate. The eigenvectors indexed between 1-100 corresponding to the dominant space of $\mathbf{V}$ have high correlations with eigenvectors indexed out past 70 of $\tilde{\mathbf{V}}$. When the communication waveforms are generated at the tag, only the eigenvectors indexed between 1-50 will be projected out with the dominant projection approach, resulting in waveforms that are less matched with the

decorrelating filters used by the receiver and more correlated to the ambient scattering interference. Looking at the plot, there also appears to be a 'loop' of correlation where eigenvectors from $\tilde{\mathbf{V}}$ have high correlations with eigenvectors at two indexes in $\mathbf{V}$. This appears to be caused by some sort of aliasing due to $\tilde{\mathbf{V}}$ having less eigenvectors than $\mathbf{V}$.

3.3 SAMPLING RATE DIFFERENCES

Another situation that can cause a mismatch between the communication waveforms generated by the tag and receiver is a difference in sampling rate when sampling the incident radar waveform $s(t)$. If the tag has a different sampling rate, it would have a different oversample factor $\tilde{M}$ than the value M at the receiver. The sampled radar waveform vector $\tilde{\mathbf{s}}$ would then be of length $N\tilde{M}$ and would be used to generate the $N\tilde{M}\times(2N\tilde{M}-1)$ scattering matrix $\tilde{\mathbf{S}}$. The communication waveforms $\tilde{\mathbf{c}}_k$ would then be generated by the set of eigenvectors $\tilde{\mathbf{V}}$ from $\tilde{\mathbf{S}}\tilde{\mathbf{S}}^H$. To simulate the mismatch in sampling rates, the receiver will have a constant oversample factor of $M=2$. The sample rate at the tag is varied from $\tilde{M}=1.6$ to $\tilde{M}=2.4$ in 0.2 steps. We will again use a P3 radar waveform of length $N=100$ and generate $K=4$ communication waveforms using the size of the non-dominant space as $\tilde{L}=(\tilde{M}-1)N$.

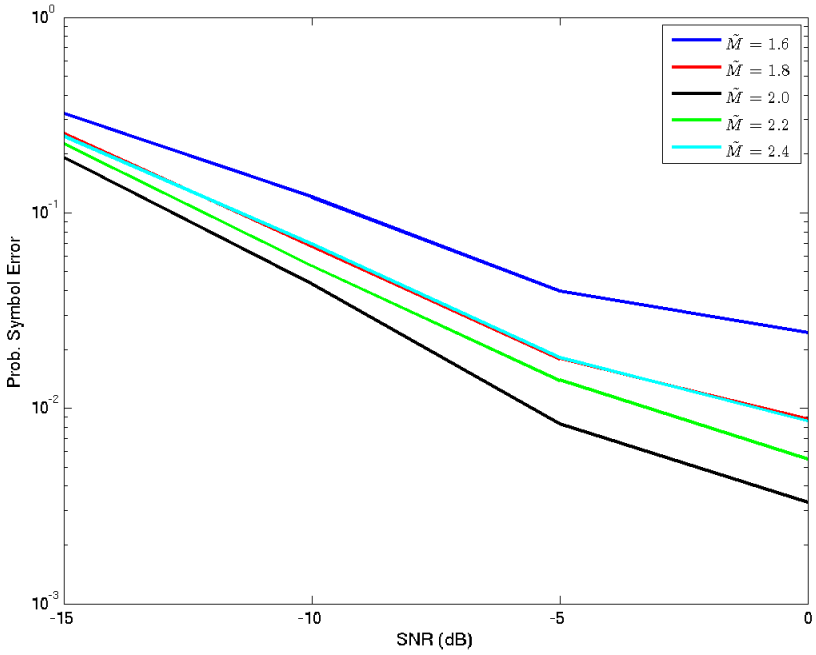

Figure 3.3.1: SER curves of sampling rate difference with Dominant-Projection

Consistent with the results in the previous sections, both the Eigenvectors-as-Waveforms and Weighted-Combining approaches are unusable with any mismatch between $\tilde{M}$ and M. For brevity, these plots are omitted as they are similar to figures 3.2.1 and 3.2.2. For Dominant-Projection, the SER results are shown in figure 3.3.1. Here, we see that the probability of symbol error goes up with a lower oversample factor of $\tilde{M} = 1.8$ and gets even worse when decreased to $\tilde{M} = 1.6$. For a higher sampling rate with $\tilde{M} = 2.2$, there is a slight increase in SER performance that further increases when $\tilde{M} = 2.4$. Dominant-Projection then appears fairly robust to sample rate differences, but is more affected by the tag using a lower sample rate than a higher sample rate.

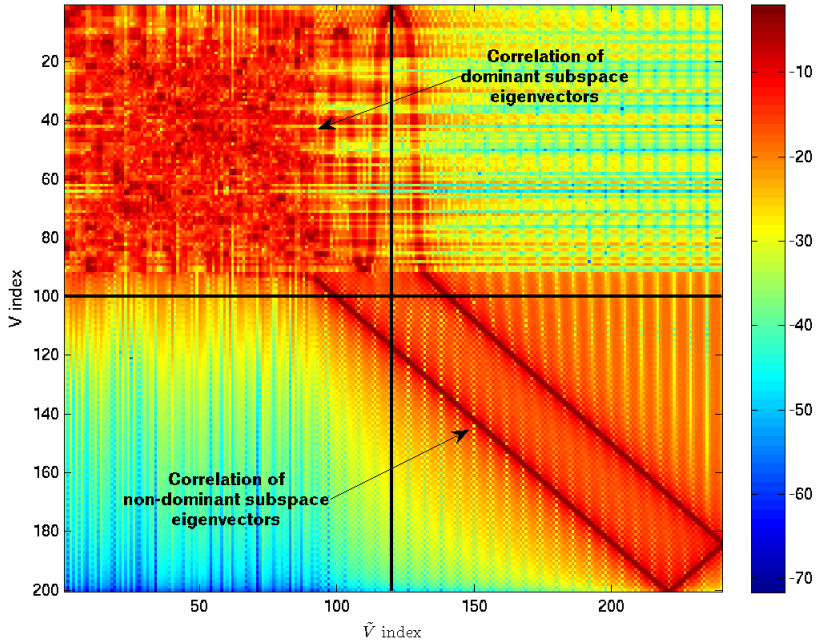

Figure 3.3.2: Eigenvector correlation with $M=2$ *and* $\tilde{M}=2.4$.

We again look at the intensity plots for the eigenvector correlation $|\tilde{\mathbf{V}}^{\mathrm{H}}\mathbf{V}|$ to gain a better understanding of the effect of different sample rates between the tag and receiver on the eigenvectors used to generate the symbol waveforms. Again, the rows for shorter of $\mathbf{V}$ and $\tilde{\mathbf{V}}$ are zero padded in order to perform the inner product operation for the correlation matrix. The eigenvector correlation intensity plot for $\tilde{M}=2.4$ is shown in figure 3.3.2 and for $\tilde{M}=1.6$ in figure 3.3.3 below. In both plots, we again see the smearing of the eigenvectors that causes the Eigenvectors-as-Waveforms and Weighted-Combining approaches to fail. For the higher sampling rate of $\tilde{M}=2.4$, we see that the dominant and non-dominant spaces are mostly separate, but the size of the non-dominant space would be $\tilde{L}=(\tilde{M}-1)\times N=140$ and the eigenvectors indexed between 1-100 would correspond to the dominant space. From

figure 3.2.2, we see that the correlations smear out past index 100. These are components that will not be projected out during the waveform generation process. The symbols generated by the tag will be less correlated with the waveforms generated by the receiver and more correlated with the clutter interference. This will causes the SER degradation that is seen in figure 3.3.1. In the eigenvector correlation intensity plot for $\tilde{M}=1.6$ shown in figure 3.3.3 below, there is even more smearing of the eigenvectors between the dominant and non-dominant spaces. This leads to the further SER performance degradation seen in figure 3.3.1.

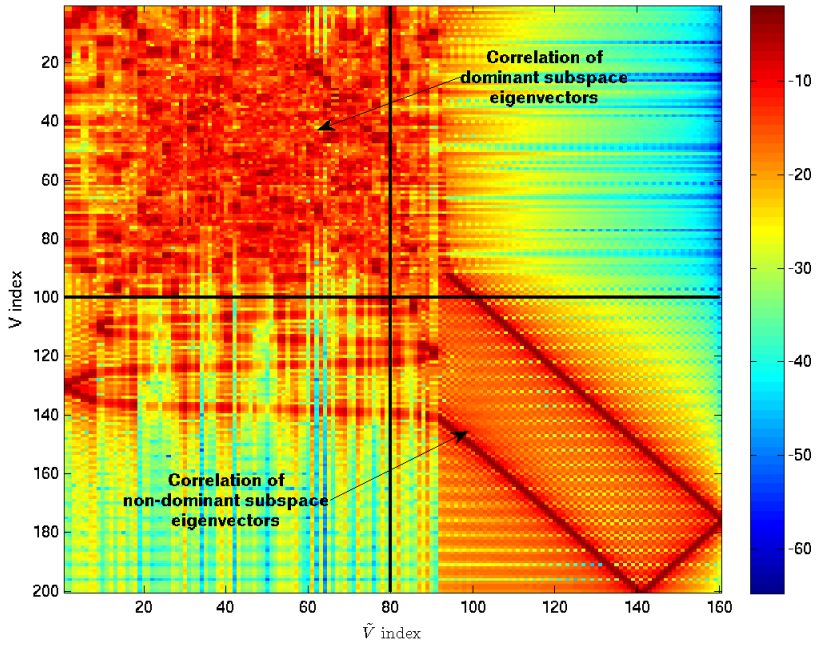

Figure 3.3.3: Eigenvector correlation with $M=2$ *and* $\tilde{M}=1.6$

CHAPTER 4

SYNCHRONIZATION ISSUES

In the previous analysis evaluating the symbol error rate performance of the waveforms for intra-pulse radar embedded communication, it was assumed that the tag and receiver were synchronized. This meant that the receiver had exact knowledge of the time that the communication waveform was received from the tag. In a real-world scenario, the receiver may not know the time delay from the tag and must search in time for the communication waveforms. For example, if the receiver is in the radar and a mobile tag is in the illuminated field, the receiver may need to search over multiple range cells to extract the embedded symbol waveform. In continuous time, this time delay of the communication waveform from the tag as seen by the receiver is

$$r(t) = c_k(t-\tau) + s(t) * x(t) + v(t) \tag{4.1}$$

where $c_k(t-\tau)$ is the transmitted communication waveform offset in time by τ, $s(t) * x(t)$ is the local clutter generated from the radar waveform $s(t)$ convolved with the clutter range profile $x(t)$, and $v(t)$ is additive white Gaussian noise. At the receiver, $r(t)$ is sampled at time i to form the vector

$$\mathbf{r}_i = \mathbf{c}_{k,i-\tau} + \mathbf{S}\mathbf{x}_i + \mathbf{v}_i \tag{4.2}$$

where $\mathbf{c}_{k,i-\tau}$ is the sampled communication waveform offset in time by τ, the matrix $\mathbf{S}$ is composed of the shifts of the sampled radar waveform vector $\mathbf{s}$ as in

equation (3.1), $\mathbf{x}_i$ is sampled local clutter range profile, and $\mathbf{v}_i$ is the additive white Gaussian noise. The receiver detects which symbol was sent by taking the maximum output of the decorrelating filter over some search period. This is described mathematically as

$$\hat{k} = \arg\left\{ \max_{k} \left\{ \max_{-\tau_{max} \le i \le \tau_{max}} \left(\left| \mathbf{w}_k^H \mathbf{r}_i \right| \right) \right\} \right\} \tag{4.3}$$

where $\mathbf{w}_k$ is the decorrelating filter for the k^{th} symbol and τ_{max} is the maximum offset for the symbol waveform.

In this chapter, we will simulate a receiver that is not synchronized with the tag and thus is required to search in time for each symbol. Again, a P3 radar waveform of length $N = 100$ is used oversampled by a factor of $M = 2$. The tag and receiver are presumed to have the same $K = 4$ communication waveforms $\boldsymbol{c}_k$ generated using the Dominant-Projection approach, each of length $MN = 200$. To approximate the continuous nature of the waveform between the tag and receiver, each communication waveform is interpolated by a factor of $M_c = 10$. The waveform is then offset randomly by τM_c, which is uniformly distributed between $[-\tau_{max} M_c, \tau_{max} M_c]$. The interpolated and time offset communication waveform is then down sampled by $M_c = 10$ to form the vector $\mathbf{c}_{k,i-\tau}$ that is added to the random clutter and noise as in equation (4.2) to generate the received waveform $\mathbf{r}_i$. The receiver detects the symbol sent by the tag by using the decorrelating filters with the maximum output over $-\tau_{max} \le i \le \tau_{max}$. This process performed over 10,000

Monte Carlo simulations of symbol transmission with random time delays and the symbol error rate is calculated.

4.1 SER PERFORMANCE SEARCHING OVER TIME

The SER results of simulations with $\tau_{max}=0,1,3,5,10$ samples are shown in figure 4.1.1. As a baseline, the SER curve with $\tau_{max}=0$ samples represents the case where the receiver is synchronized with the waveform from the tag. With $\tau_{max}=1$ sample the match point of the communication waveform in $\mathbf{r}_i$ has an offset that is uniformly distributed between $-1 \le i \le 1$ in steps of $1/M_c=0.1$ samples.

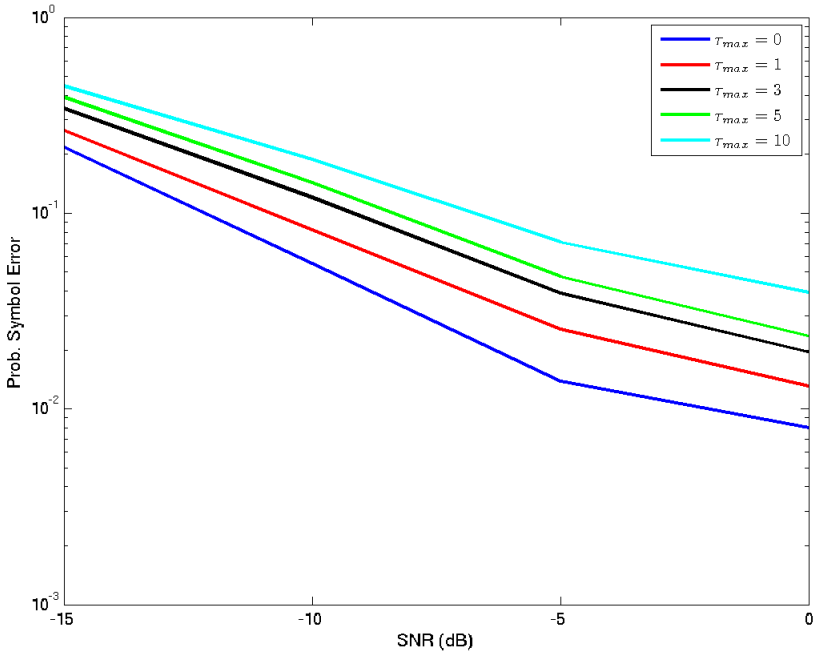

Figure 4.1.1: SER of Dominant-Projection searching over τ_{max} samples.

Here, we see as τ_{max} is increased, the SER performance degrades. In other words, the more samples that the receiver must search increases the chance that an

error will occur. In the next two sections we will attempt to reduce the amount of errors caused by the receiver searching over time because of a lack of synchronization with the tag.

4.2 THREE SAMPLE AVERAGE

The first attempt at improving SER performance when the tag and receiver are not synchronized comes about from looking at the autocorrelation of the communication waveforms generated with the Dominant-Projection approach. The autocorrelation plots for each of the four symbol waveforms are shown in figure 4.2.1.

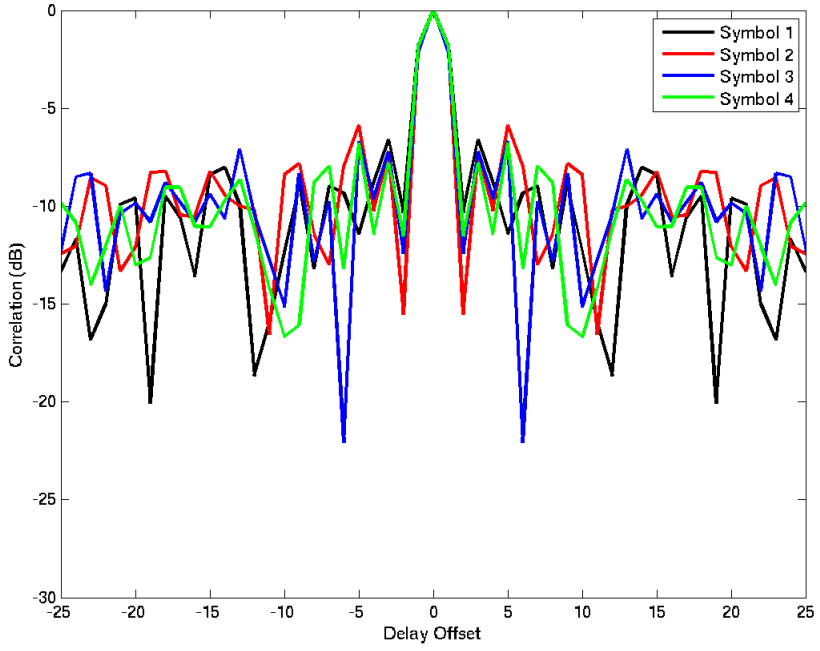

Figure 4.2.1: Autocorrelation of Dominant-Projection communication waveforms.

In the autocorrelation for each symbol, at delay offsets of +/- 1 the correlation is just 2-3 dB down from the match point (0 offset). Intuitively, it seems that it may be possible to average over three samples to take advantage of this width in the autocorrelation. Noise and interference that may cause a symbol error at one sample offset in the receiver may be averaged out over three samples, thereby reducing symbol errors. The receiver would then average the output of equation (4.2) as

$$\hat{\mathbf{r}}_i = \frac{1}{3}(\mathbf{r}_{i-1} + \mathbf{r}_i + \mathbf{r}_{i+1}) \tag{4.4}$$

and then used in equation (4.3) to detect the embedded waveform.

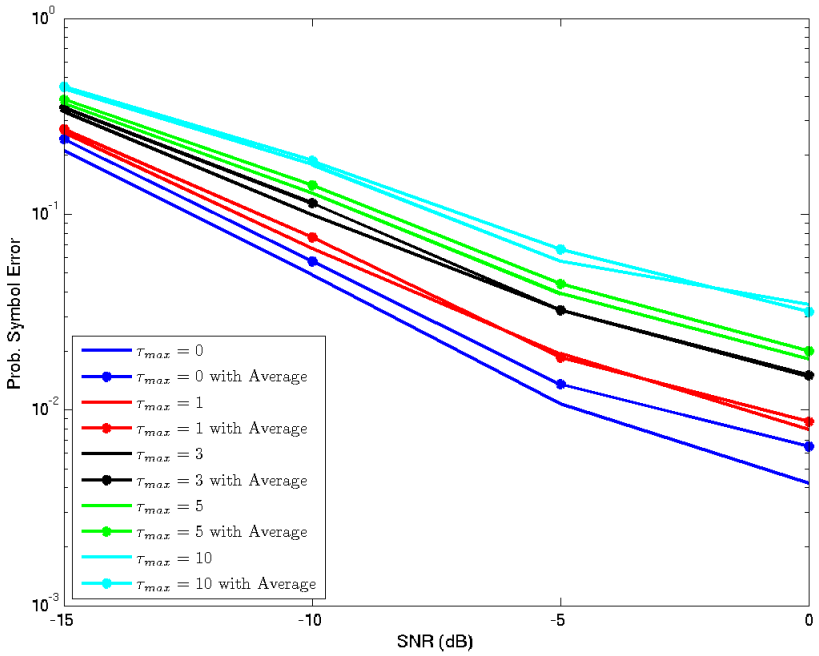

Figure 4.2.2: SER searching over time and averaging 3 samples.

Monte Carlo simulations were run with and without the three sample average with the receiver searching over the same range values of τ_{max} as in section 4.1. The

SER results for the simulation are shown in figure 4.2.2. Here, we see that the three sample average does not seem to improve SER performance of the receiver. Actually, in the majority of data points, the average slightly increases the probability of symbol error. The output of the decorrelating filters at plus and minus one sample from the match point do not appear to contain any more information for detecting the communication waveform and may instead introduce more noise and interference. This would then cause an increase in the probability of symbol error. This is further examined later in section 4.4.

4.3 SYMBOLS WITH LESS LOCAL CROSS-CORRELATION

The second attempt to improve the SER performance when the receiver searches over multiple samples comes about from examining the cross-correlations of the symbol waveforms generated with the Dominant-Projection approach. In figure 4.3.1, the cross-correlation between each symbol waveform with the first symbol is shown.

In these plots, we see that the correlation between the first waveform and the three other communication waveforms goes down to about -40 dB at the match point. This null results from the Dominant-Projection approach; since the dominant eigenvectors and each previously generated communication waveform are projected away from the random seed vector, the resulting new waveform will be less correlated with any previously generated waveform at the match point.

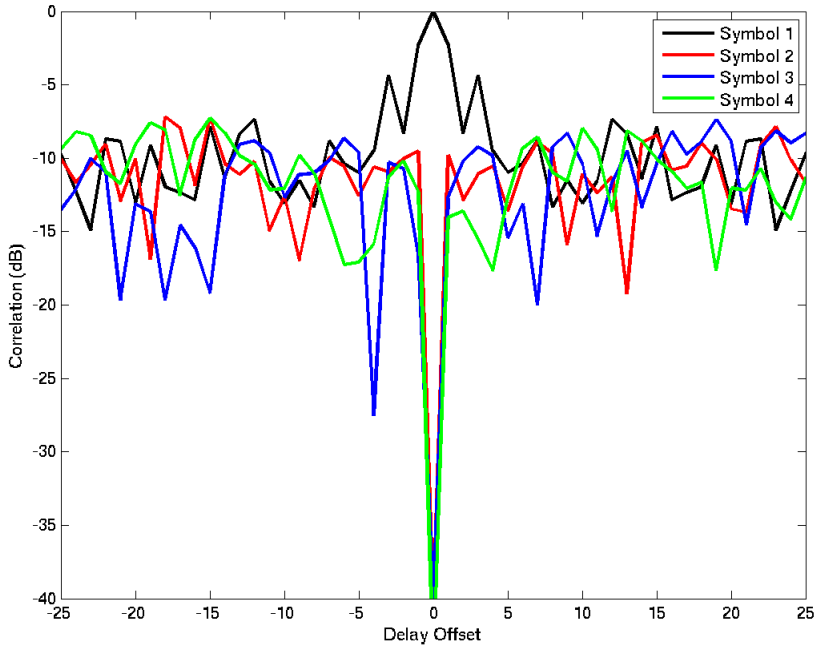

Figure 4.3.1: Cross-correlation of communication waveforms.

If, instead of just projecting away from the previously generated communication waveforms at their match point, shifted versions of the waveforms are also projected out, communication waveforms can be generated with lower cross-correlation local to the match point. This changes equation (2.6) in the Dominant-Projection approach to

$$\mathbf{S}_k = [\mathbf{S}\ \mathbf{C}_1 \ldots \mathbf{C}_{k-1}]\,. \tag{4.5}$$

where the $2f+1 \times MN$ matrix

$$\mathbf{C}_k = \begin{bmatrix} c_{k,f} & \cdots & c_{k,0} & \cdots & 0 \\ c_{k,f+1} & \cdots & c_{k,1} & \cdots & \vdots \\ \vdots & \ddots & \vdots & \vdots & c_{k,NM+f-2} \\ 0 & \cdots & c_{k,NM-1} & \cdots & c_{k,NM+f-1} \end{bmatrix} \tag{4.6}$$

contains the $2f+1$ shifted versions of the communication waveform $\mathbf{c}_k=[c_{k,0}\ c_{k,1}\ \ldots\ c_{k,MN-1}]^T$.

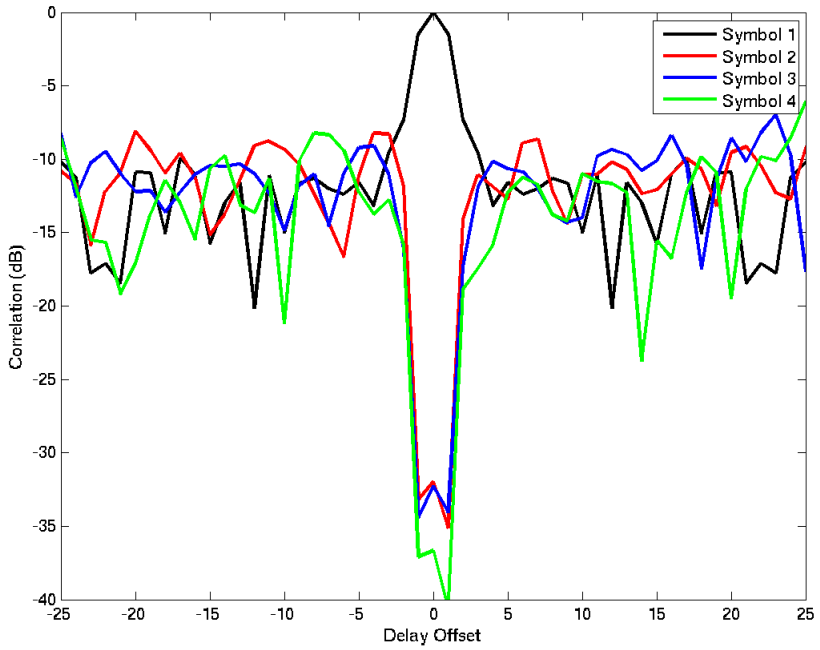

Figure 4.3.2: Dominant-Projection with less local cross-correlation.

Communication waveforms were generated with the Dominant-Projection approach including the delay shifts of -1, 0, and +1 ($f=1$) of each of the previously created waveforms in the projection matrix. The cross-correlation plots of the resulting symbol waveforms are shown in figure 4.3.2. From these cross-correlations, we see that projecting away the delay shifts of the previously generated waveforms has the desired effect of widening the null near the match point, but the null is not quite as deep as the waveforms generated without the shifts included.

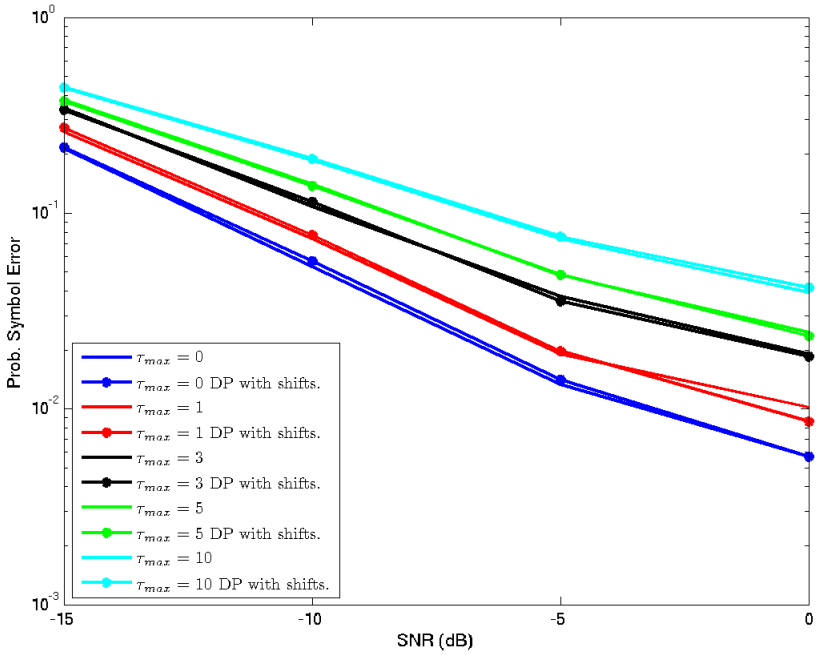

Figure 4.3.3: SER of Dominant-Projection with local cross-correlation, searching over time.

Monte Carlo simulations were again run comparing the probability of symbol error when using the communication waveforms generated with the lower local cross-correlation with symbols generated with the original Dominant-Projection method. From the SER curves shown in figure 4.3.3, we see that the waveforms with lower local cross-correlation do not appear to perform better in terms of symbol error rate. As with the three sample average, at many of the data points, the waveforms generated to have less local cross-correlation actually have a slightly higher probability of symbol error in comparison to the waveforms generated with the regular dominant projection approach. This will be further explored in the next section.

4.4 DISTRIBUTION OF FILTER OUTPUTS

In the last two sections, attempts were made to improve the SER performance using the Dominant-Projection approach when the receiver is not synchronized with the tag waveform and must search over a number of samples to detect the embedded communication waveform. The proposed improvements included using a three sample average of the filter outputs to take advantage of the width of the autocorrelation of the communication waveforms as well as reducing the local cross-correlation of the waveforms by projecting away shifts of the previously generated waveforms when using the Dominant-Projection approach. In this section, we will examine the distribution of the output magnitude of the decorrelating filter as an estimate of each filter output's probability density function (pdf). This is done in order to gain a better understanding of the causes behind symbol errors that are occurring and some reasons these two approaches fail to reduce the number of errors.

Recall that the receiver uses the filter with largest output magnitude to determine which symbol was sent by the tag as in equation (4.3). A symbol error will occur when the output of one of the other three filters is larger than the filter corresponding to the symbol that was actually sent (i.e. $\hat{k} \neq k$). Therefore, estimating the probability density function (pdf) of each filter output ($|\mathbf{w}_k^H \mathbf{r}_i|$) can give a better understanding of the effect of interference and noise in causing symbol errors. Also, the effect on the pdfs from the attempts to improve SER performance from the previous two sections can be observed and give more information as to why the approaches were not effective.

To approximate the pdfs of the decorrelating filter outputs, 10,000 Monte Carlo simulations are run with the tag sending the first generated symbol. The symbol is added to random clutter and noise as in equation (4.2), the output magnitude of each decorrelating filter ($|\mathbf{w}_k^H \mathbf{r}_i|$) for $i = -1, 0, 1$ is computed and a histogram of the output magnitude values is generated with 25 bins for values ranging from 0 to 2. The histogram is then plotted as a line plot as an estimate of the pdf for each decorrelating filter output magnitude.

Figure 4.4.1 shows the estimated probability density function plots of the output magnitude for each decorrelating filter with -35 dB SIR and -5 dB SNR at the match point of the symbol waveform (i.e. tag and receiver synchronized). Here, we see that the distribution of the output magnitude of the filter for the transmitted symbol (symbol 1) is clearly distinguishable and set apart from the other three symbols (symbols 2-4). The more that the transmitted waveform can be separated from the other possible waveforms, the less probability of a symbol error. The mean output magnitude of the filter for symbol 1 is around 1.0. The value near unity is attributed to match between the tag waveform and the decorrelating filter used by the receiver. The magnitude of the filter output varies from the clutter and the noise with a standard deviation of 0.23. The mean output magnitude for the decorrelating filters for the other three symbols is each around 0.27 with a standard deviation of 0.14. Recall that the communication waveforms are designed to be partially correlated with ambient scattering to have a low probability of intercept; therefore, each filter will be partially correlated with the received clutter interference.

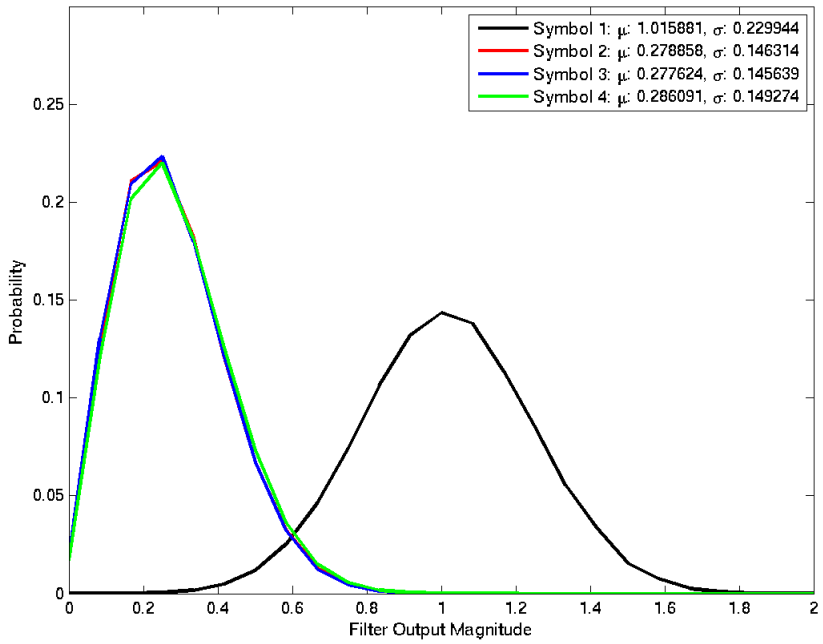

Figure 4.4.1: Estimated pdfs of Dominant-Projection reception.

If only two communication waveforms were used, the overlap of the pdfs between symbol 1 and symbol 2 in figure 4.4.1 would give a good indication of the probability of symbol error, given an error occurs when the output magnitude of the filter corresponding to symbol 2 is larger than the magnitude of symbol 1 filter (with symbol 1 being sent). With four symbols, an error will occur when the output of any of the other three decorrelating filters has a larger magnitude than the output of the filter corresponding to the actual embedded symbol. The pdfs of the three other filter outputs must be combined and compared to the pdf for the symbol sent. Since it is the largest magnitude of the three other filter outputs that will cause an error, the pdf of maximum value of the filters for symbols 2-4 will be generated and compared to the estimated pdf for symbol 1.

Figure 4.4.2 shows the estimated pdf of the largest output magnitude of the decorrelating filters for symbols 2-4 with the pdf for the symbol 1 filter. From the plot, we see that the combination of the three individual pdfs from figure 4.4.1 by taking the maximum value, increases the mean to about 0.40 from about 0.27 individually. There is also only a very slight decrease in standard deviation. This increase in the mean value pushes the pdf of an erroneous symbol further into the pdf of the correct symbol, increasing the probability of symbol error. This would be a major contributer to the decrease in SER performance when increasing the number of symbols K used in the system. With more symbols, there are more possibilities for the magnitude of a decorrelating filter corresponding to a symbol that was not sent to have a larger magnitude than the filter for the correct symbol, causing a symbol error.

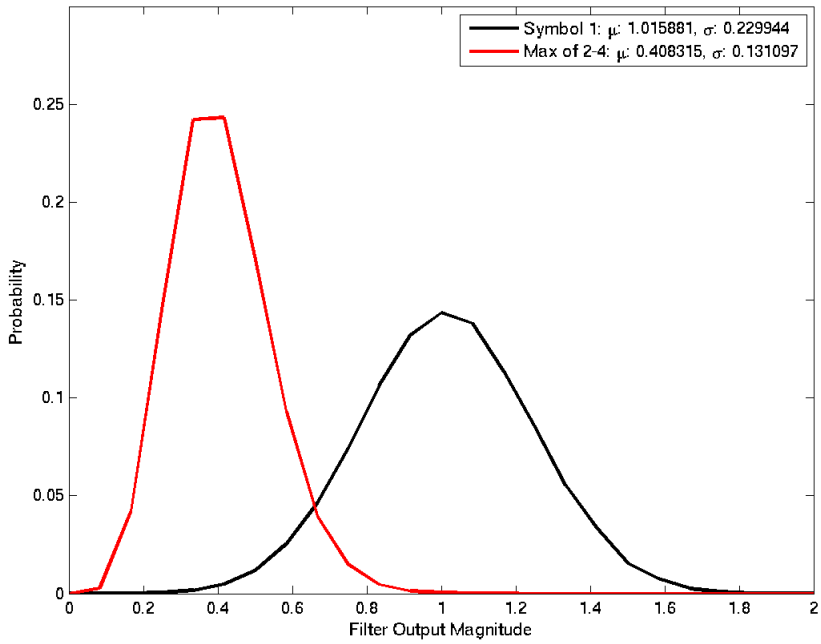

Figure 4.4.2: Estimated pdf of Dominant-Projection detection.

When the receiver is not synchronized with the tag, it must search over multiple samples to find the symbol waveform that was sent. In this case, the receiver takes the largest filter output over the samples searched. That means at any sample offset searched, if any of the decorrelating filters for the three other symbols not sent by the tag is larger than the largest filter output of the symbol that was sent, a symbol error occurs. Figure 4.4.3 shows the resulting pdfs when searching over three samples, corresponding to the $\tau_{max}=1$ SER curve from figure 4.1.1. From the plot, we see that the mean of the largest competing symbol that would cause an error increases to about 0.51. This is up from about 0.42 of the synchronized case in figure 4.4.2. The increased overlap between the error symbol and correct symbol illustrates the degradation in SER performance seen when searching over the three samples.

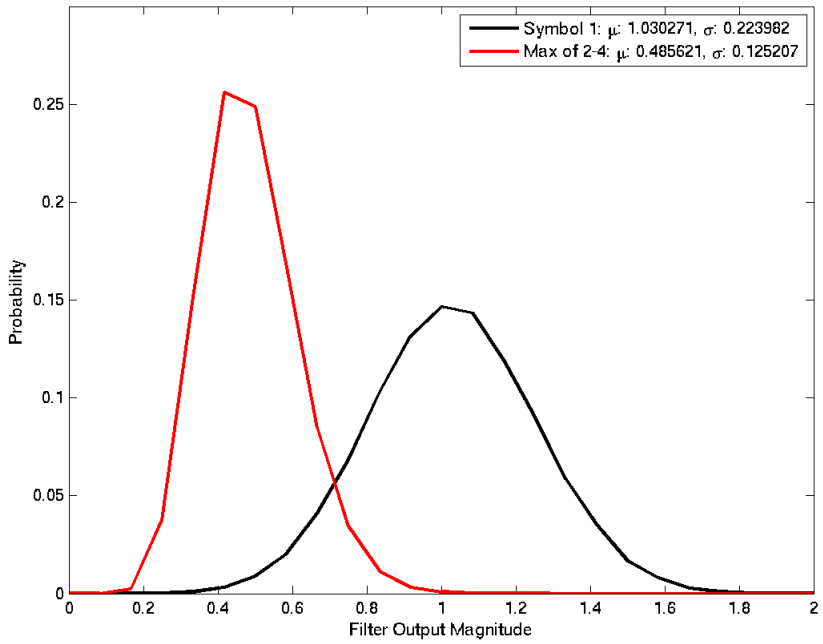

Figure 4.4.3: Estimated pdf with searching in time +/- 1 sample.

In section 4.2, a three sample average of each filter output was used in an attempt to improve SER performance when searching over multiple samples. Since the autocorrelation of the symbol waveforms at +/- one sample is just 2-3 dB down from the match point, an average over those three samples was thought to be able to reduce symbol errors. In figure 4.4.4, we see the effect of a three sample average on estimated pdfs for the decorrelating filter outputs for symbol 1 and the maximum of symbols 2-4. The pdfs are shown at the match point, offset by +/- 1 sample, and the three sample average.

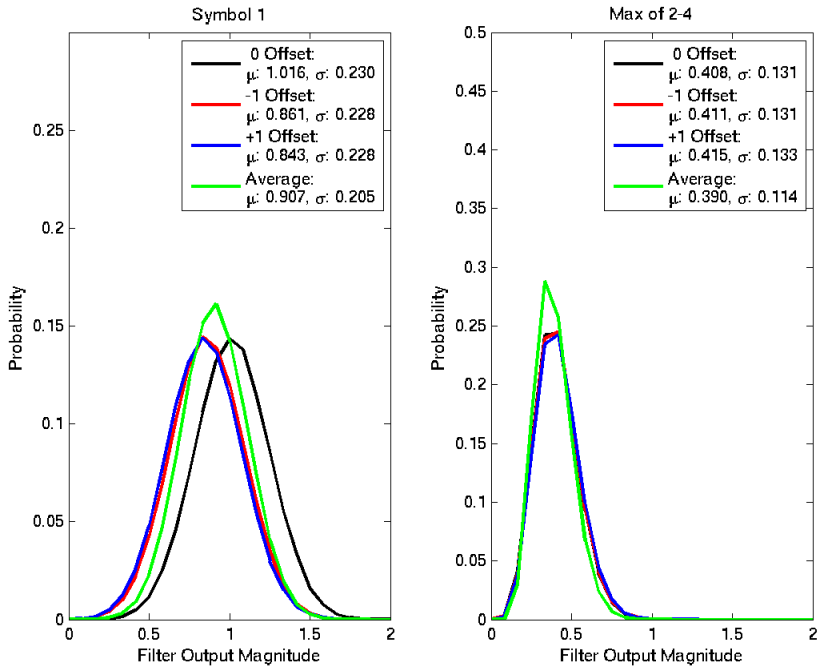

Figure 4.4.4: Estimated pdf for Dominant-Projection at three sample offsets and with average.

From the plot, we see that the three sample average reduces the standard deviation of the filter output for symbol 1, but since the correlation at +/-1 sample

from the match point is down 2-3 dB, the average over these samples also reduces the mean of the distribution. The pdf for the maximum filter output for symbols 2-4 shows a slight decrease in both the mean and standard deviation.

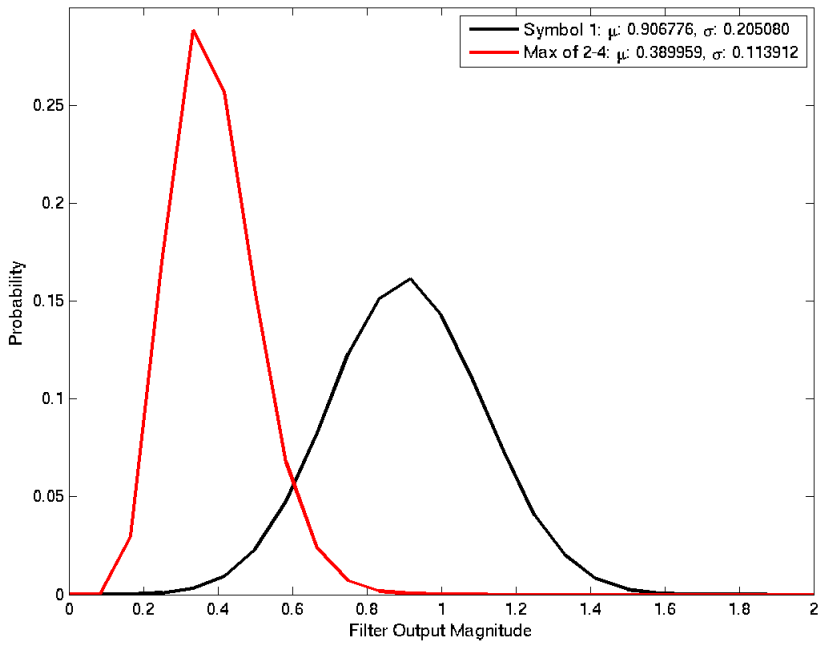

Figure 4.4.5: Estimated pdf for DP with three sample average detection.

The distributions resulting from the three sample average of the filter outputs are shown in figure 4.4.5. These plots correspond to the SER curve in figure 4.2.2 with $\tau_{max}=0$. Here, we see that the pdf of the maximum of the three sample average for symbols 2 – 4 has a mean that decreases from 0.43 without the three sample average to about 0.41. But, with the decrease in the mean for symbol 1 from 1.01 to about 0.93 and without a significant reduction of the variance, resulting in the two distributions moving closer together. This slight increase in the overlap of the two distributions matches the slight increase in the probability of symbol error that was

observed in figure 4.2.2.

In section 4.3, the symbol waveforms were generated to have less local cross-correlation with the other symbols in an attempt to improve SER performance. This was accomplished by projecting away shifts of the previously created waveforms along with each symbol at the match point in the Dominant-Projection procedure. The thought is that the lower correlation between waveforms at small offsets would reduce the chance of symbol error when the receiver searches over multiple samples for the waveform from the tag.

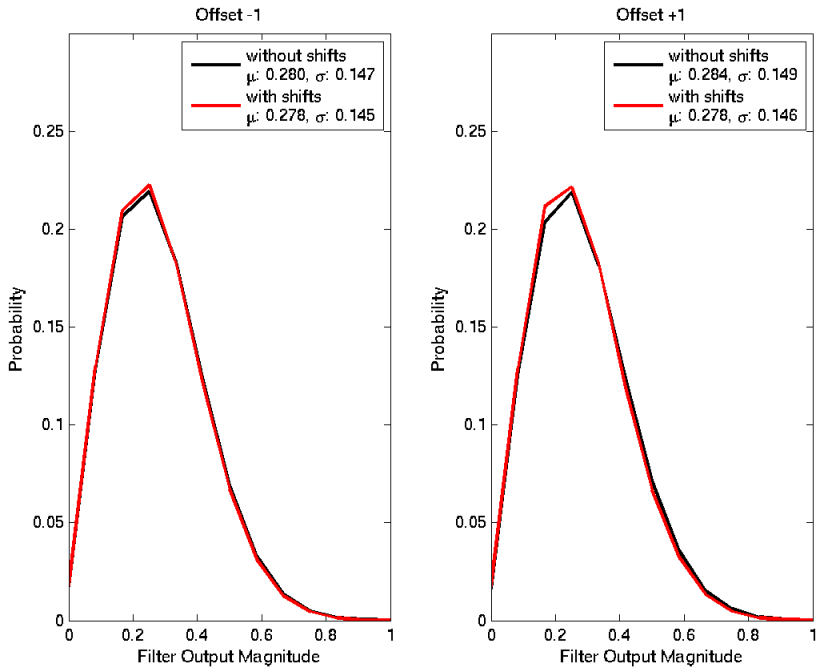

Figure 4.4.6: Estimated pdf DP with lower local cross-correlation.

Figure 4.4.6 compares the distributions of the decorrelating filter output magnitude for the Dominant-Projection symbols generated with and without the shifted versions of the previously generated symbols included in the projection to

generate new symbols. The distribution of the filter output for symbol 2 at +/- 1 sample delay from the synchronization point is shown with the tag transmitting symbol 1. To improve SER performance, the lower-cross correlation should reduce the outputs of the other three filters one sample off the match point. Here, we see that the lower local cross-correlation only slightly reduces the mean and standard deviation of the filter output for symbol 2. Similar results are seen for the other two symbols.

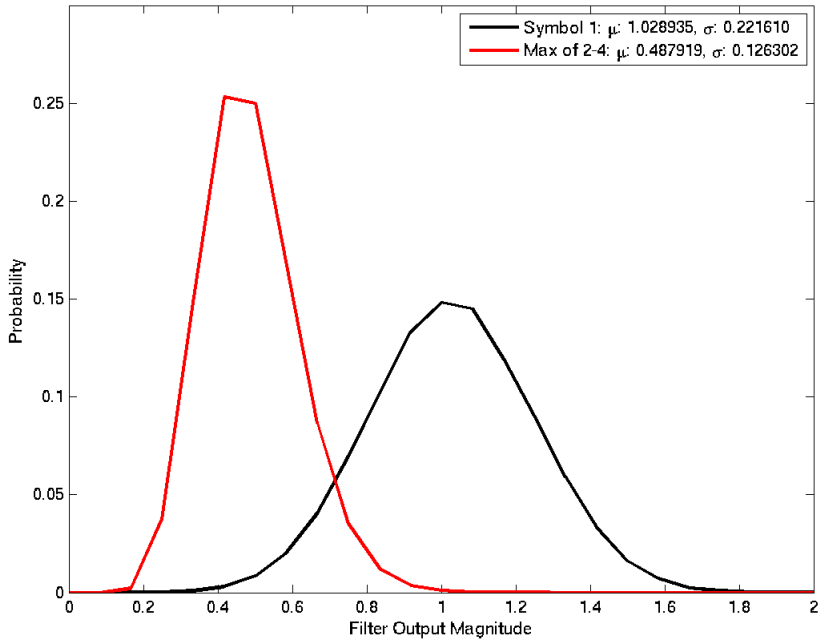

Figure 4.4.7: Estimated pdf DP with lower local cross-correlation.

In figure 4.4.7, we see the pdfs of the transmitted waveform (symbol 1) and the maximum of the other three waveforms with the Dominant-Projection approach with the inclusion of the shifted communication waveforms used to achieve lower local cross-correlation between the symbols. Here, we see that the distributions are

not significantly different than resulting pdfs when using symbols generated by the original dominant projection approach, as shown in figure 4.4.3. As seen in the SER curve in figure 4.3.3 with $\tau_{max}=1$, the lower local cross-correlation does not appreciably reduce the probability of symbol error.

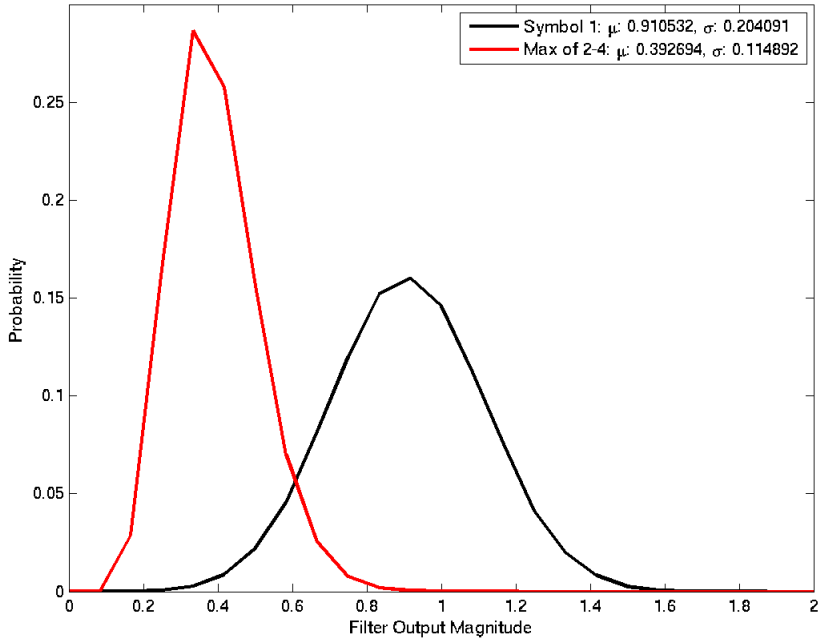

Figure 4.4.8: Estimated pdf DP with lower local cross-correlation and average.

In figure 4.4.8, the two approaches from sections 4.2 and 4.3 are combined such that the communication waveforms are generated with lower local cross-correlation used with the receiver using a three sample average of the filter outputs. Here, we see that the pdfs of the transmitted symbol and the maximum of the three other symbols are not significantly improved by the combination of the two approaches; therefore, a decrease in SER is not anticipated from the combining of the

two approaches.

4.5 MULTIPATH AND SYNCHRONIZATION

In section 3.1, multipath distortion of the radar signal between the transmitter and the tag was considered. In the simulations, the sampled version of the multipath distorted radar waveform was used by the tag to generate the communication waveforms, but the symbols did not encounter a multipath channel from the tag to the receiver. If the receiver is co-located with the transmitter, by reciprocity, the communication signal should encounter the same multipath channel from the tag back to the receiver. In this section, we will test the symbol error rate performance when the communication waveforms are distorted by multipath between the tag and receiver.

In section 3.1, it was shown that the Dominant-Projection waveform design approach was robust to multipath distortion, generating correlated symbol waveforms even under severe multipath conditions. For the simulations in this chapter, the sampled radar waveform vector $\mathbf{s}$ is again distorted by the sampled impulse response of the multipath profile vector $\mathbf{h}$ such as

$$\tilde{\mathbf{s}} = \mathbf{s} * \mathbf{h} \tag{4.4}$$

where $*$ is the convolution operation. The vector $\tilde{\mathbf{s}}$ is then truncated and used by the tag to generate the $K = 4$ the communication waveforms $\tilde{\mathbf{c}}_k$ using the Dominant-Projection approach. The receiver again uses the undistorted sampled radar waveform $\mathbf{s}$ to generate the decorrelating filters $\mathbf{w}_k$ used to detect the symbols

sent by the tag. The symbol waveforms are distorted by the same multipath profile $\mathbf{h}$ such that the signal sampled at the receiver $\mathbf{r}$ is given by

$$\mathbf{r} = \tilde{\mathbf{c}}_k * \mathbf{h} + \mathbf{S}\,\tilde{\mathbf{x}} + \mathbf{v} \tag{4.5}$$

where the result of the convolution $\tilde{\mathbf{c}}_k * \mathbf{h}$ is truncated to length NM, $\tilde{\mathbf{x}}$ is a length $2NM-1$ vector of the radar range profile of the clutter and $\mathbf{v}$ is NM samples of additive noise.

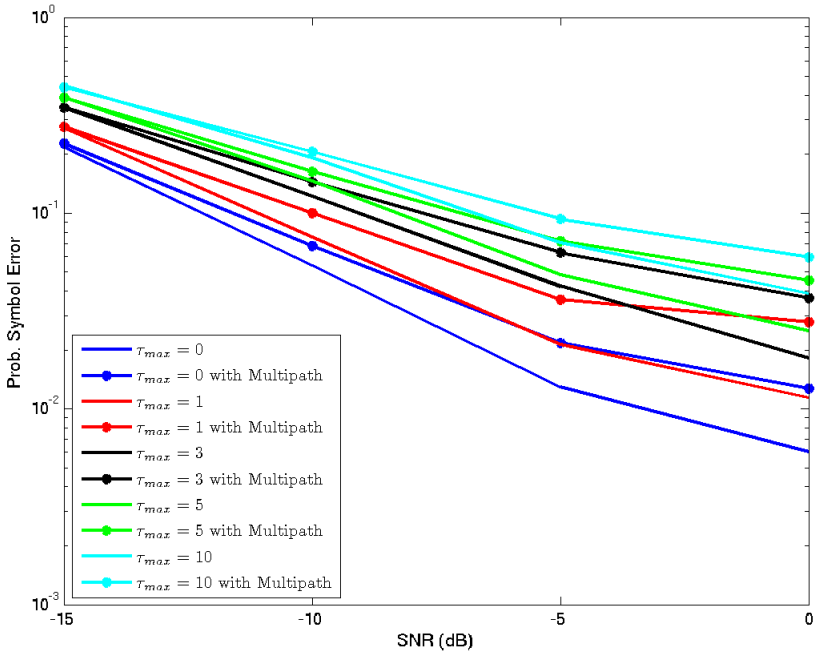

Figure 4.5.1: SER performance with and without multipath distortion from -10 dB AWGN with the receiver searching over τ_{max} samples.

Figure 4.5.1 shows the SER results with the receiver searching over $\tau_{max} = 0, 1, 3, 5, 10$ samples with and without multipath distortion of an impulse with additive white Gaussian noise (AWGN) with an average power of -10 dB. This is the same multipath scenario tested in section 3.1.1 with SER results (without multipath

between the tag and receiver) shown in figure 3.1.3. While the distortion caused by this multipath profile did not cause different communication waveforms to be generated between the tag and receiver (as seen by the negligible difference in SER performance), there is a noticeable degradation in performance when the communication waveform is distorted by this multipath profile.

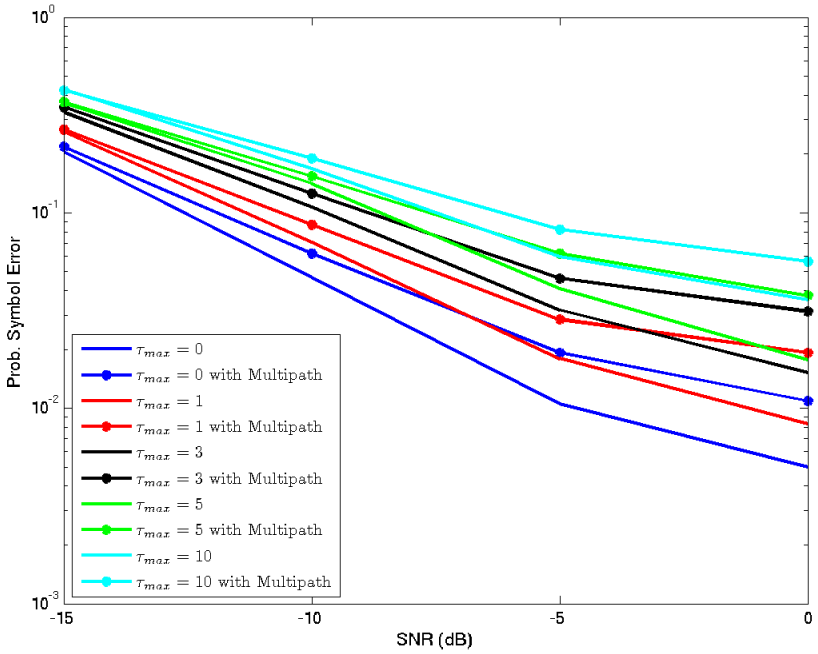

Figure 4.5.2: SER performance with and without multipath distortion from from a second random impulse with the receiver searching over τ_{max} *samples.*

Figure 4.5.2 shows the SER results when the multipath is instead caused by a second, randomly delayed impulse with a random complex amplitude as was used in section 3.1.2. Again, we see an increase in symbol errors caused by the distortion of the symbol waveform from multipath. From the SER performance of Dominant-Projection observed in figure 3.1.4, this multipath profile did not cause enough

difference in the symbol waveforms to cause an increase in errors when only applied to the radar signal between the transmitter and the tag, but does increase the probability of error when the symbol waveforms are distorted from the tag to the receiver.

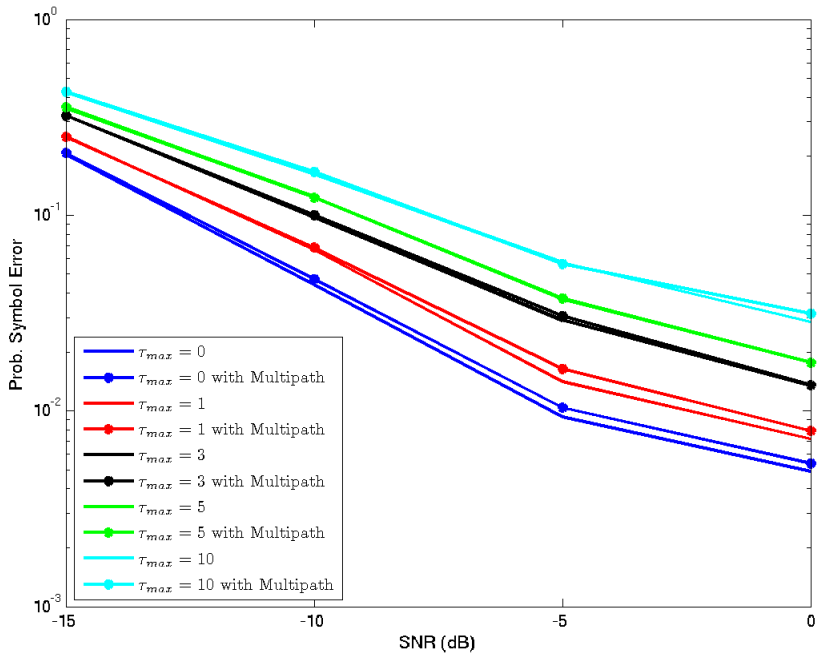

Figure 4.5.3: SER performance with and without multipath distortion from -15 dB AWGN with the receiver searching over τ_{max} samples.

Figure 4.5.3 shows the SER performance curves when the power of the AWGN is decreased to -15 dB from the -10 dB used in the simulation shown in figure 4.5.1. Here, we see that the decrease in the power of the convolved noise decreased the degradation caused by the multipath distortion. Also, in figure 4.5.4 we see that by decreasing the average complex amplitude of the impulse for the second multipath component to -7 dB from 0 dB used in figure 4.5.2, significantly decreases the

degradation caused by the distortion. From these plots, we see that the receiver is robust to moderate levels of multipath distortion of the communication waveform from the tag, but higher levels of distortion will cause an increase in the occurrence of symbol errors. More work will need to be done to improve SER performance in the presence of more significant multipath channel between the tag and receiver. If the tag can determine the channel response from the incident radar waveform, the communication waveforms could be pre-distorted such that a gain could be realized from the multipath channel. The other possibility is the receiver using deconvolution to remove the distortion as in adaptive pulse compression (APC) as in [17].

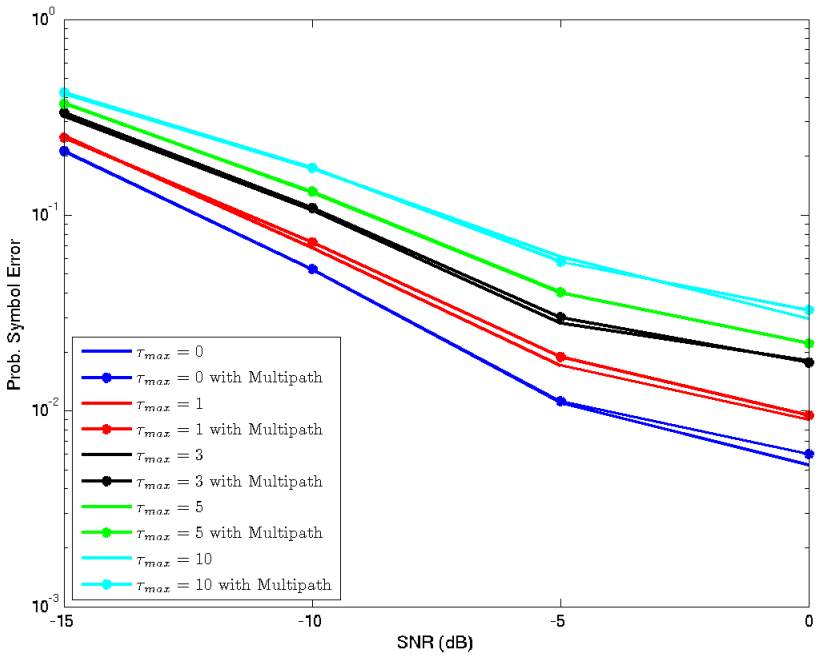

Figure 4.5.4: SER performance with and without multipath distortion from from a second random impulse with the receiver searching over τ_{max} *samples.*

4.6 INTERCEPT RECEIVER SYNCHRONIZATION

Lack of synchronization with the tag can also cause problems for an intercept receiver trying to detect any communication waveforms sent. Previously, a low probability of intercept (LPI) metric was developed to compare how well each of the original three symbol waveform generation methods remained hidden in the clutter and thus, had less probability of being detected by an unintended receiver. The LPI metric was generated by projecting away a percentage of the eigenvectors of the correlation matrix $\mathbf{SS}^H$ and calculating the normalized correlation of the result with the actual communication waveform sent. This LPI metric assumed both synchronization with the tag and that the intercept receiver knew the oversample factor M used to generate the symbol waveforms. In this section, the effect on the LPI metric of sample offsets and a larger over sample factor for the intercept receiver are simulated.

In simulating the delay offset's effect on the LPI metric, the symbol waveform is shifted by the number of delay samples and added to random interference and noise. The eigenvectors of $\mathbf{SS}^H$ are projected away one by one with the result correlated with the known symbol waveforms as a measure of the intercept receiver's ability to recover the transmitted symbol waveforms. Here, only the correlation plot of the symbol waveform sent (symbol 1) is shown to compare its LPI metric at the different sampling offsets.

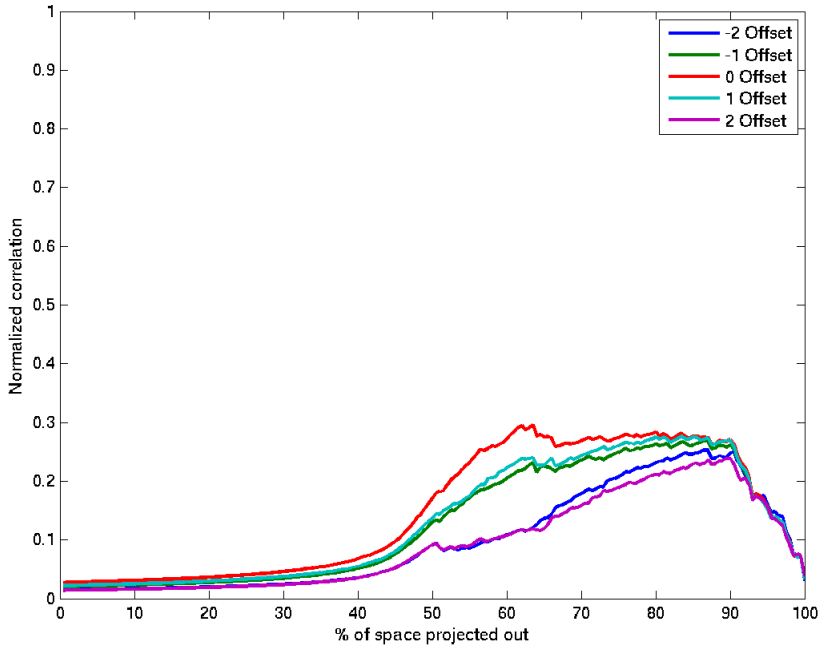

Figure 4.6.1: LPI Metric at different sample offsets.

In figure 4.6.1, the LPI metric is shown with the intercept receiver having delay offsets ranging from -2 to +2 samples. Here, we see that the peak correlation level decreases with a larger sampling offset going from about 0.30 when synchronized to about 0.25 with +/- 2 sample offset. Also, the peak correlation level for 0 offset is near 60% of the space projected out. At this point the normalized correlation values with an offset are noticeably reduced. With all of this, it appears that a lack of synchronization would make it more difficult for the intercept receiver to detect the communication waveforms sent by the tag.

Another assumption made with the previously used LPI metric is that the oversample factor used by the tag to generate the symbol waveforms is known by the the intercept receiver. If this bandwidth is not known, the intercept receiver could

instead further oversample received waveforms while searching for the communication waveforms. With the increased bandwidth, the symbol waveforms must be interpolated to the oversample factor used by the simulated intercept receiver and added to random signal and noise. The intercept receiver uses the oversampled radar waveform to generate and project out the eigenvectors of the correlation matrix $\mathbf{SS}^H$. The LPI metric is then calculated as before with the correlation of the actual waveform sent (symbol 1) compared with the other three waveforms.

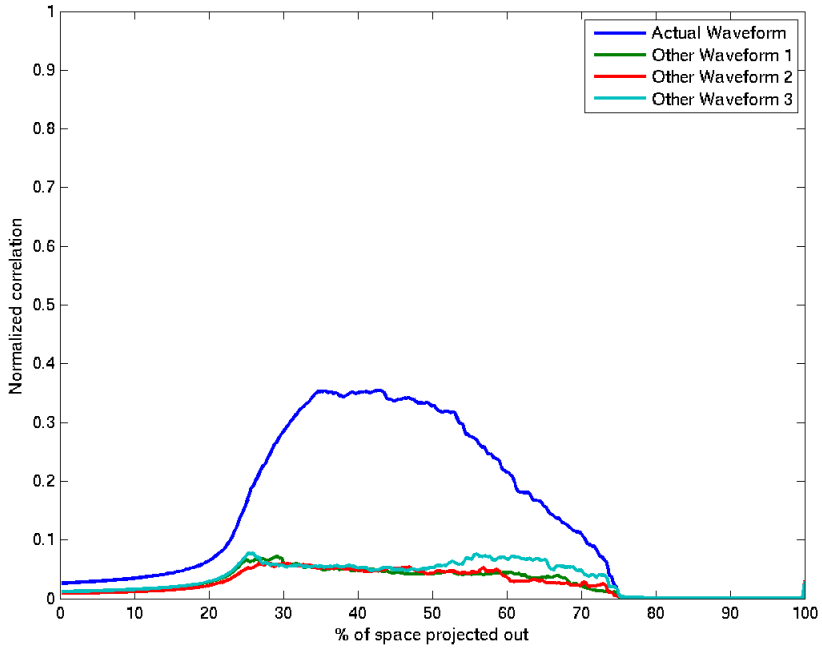

Figure 4.6.2: LPI metric with a higher sampling rate.

Figure 4.6.2 shows the LPI metric with the tag oversampling the incident radar waveform factor of $M=2$ to generate the communication waveforms and the intercept receiver using an oversample factor of $\tilde{M}=4$ to the search for the waveforms. Here, we observe that the peak correlation level of the actual waveform

present is about 0.35 and for the other waveforms it is about 0.08. The increase in peak correlation from around 0.30 seen in figure 4.6.1 may make it slightly easier for the intercept receiver to detect the communication waveforms, but there is a higher computational cost of using a larger bandwidth. The increase in sampling rate also moves the normalized correlation "hump" seen in figure 4.6.1 from about 50% to 100% of the space projected away to about 25% to 75%. Based on this and the changes in the correlation plots from sample offsets in figure 4.6.1, it may be difficult for the intercept receiver to determine the amount of space to project away to best detect the communication waveforms.

CHAPTER 5

IMPROVING WAVEFORM DESIGN

While chapters 2 and 3 dealt with issues of generating and receiving the communication waveforms, this chapter will focus on improving the symbol waveform design to reduce the probability of symbol error. By increasing the length used for the incident radar waveform (and thus, increasing the communication waveform length), each symbol should be more separable by the receiver while still remaining hidden in the ambient scattering. Also, by generating symbol waveforms that have less cross-correlation, they should be more separable by the receiver. If the symbols have different amounts of correlation with the interference, mixing them with the Hadamard Transform should equalize the correlation, leading to less errors. Lastly, adjusting the amount of correlation of the symbol waveforms with the clutter should influence SER performance; decreasing the correlation will increase performance. These four methods are further explored below.

5.1 TEMPORAL EXPANSION

For each communication waveform generation method, the spectral bleeding of the radar signal is utilized to hide the symbols for covert communication. The bandwidth of the radar waveform is expanded as an added design dimension for the communication waveforms such that they can remain hidden. As was seen in chapter 3, the multiple, delayed copies of the radar waveform caused by forward scattering

and clutter can also make it difficult to determine the length of the radar signal, making the waveform appear longer (see figure 3.2.1). The communication waveforms could then also be longer, while still being hidden by the ambient scattering. Temporal expansion may then be used along with the expanded bandwidth as an additional dimension for communication waveform design. The resulting communication waveforms achieve an improvement in SER performance.

5.1.1 SER PERFORMANCE WITH TEMPORAL EXPANSION

In section 3.2, simulations were run with the tag determining a different length for the radar waveform used in the generation of the communication waveforms. From the SER results in figure 3.2.4, when the tag used a shorter length, the probability of symbol error increased, but when a longer length was used, there was not a significant difference in probability. It would seem that the increased SER with the tag using a shorter waveform length would be unchanged if the receiver also used the shorter length and if the receiver and tag both use the longer waveform length the SER would improve. Monte Carlo simulations were then run again as in section 3.2, but in this case both the tag and receiver use the same value $\tilde{N}$ for the sampled incident radar waveform.

The SER performance from the simulations with the tag and receiver both using radar waveform lengths of $\tilde{N} = 100, 110, 130, 150$ used with the Dominant-Projection approach to generate the communication waveforms is shown in figure 5.1.1. From the SER curves, we observe that the probability of symbol error is significantly decreased with each increase in the length of the radar waveform. The

length could then be increased based on the ambient scattering to improve the SER while remaining LPI.

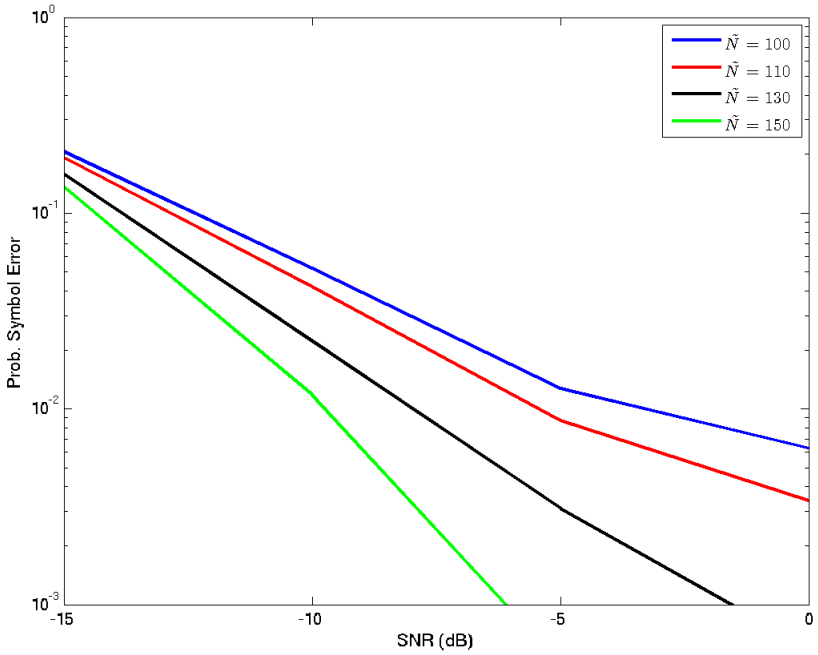

Figure 5.1.1: SER Performance Increases with Increasing Radar Waveform Length

5.1.2 ADDED DIMENSIONALITY OF TEMPORAL EXPANSION

Increasing the length of the sampled radar waveform used in the communication waveform generation process adds extra dimensionality for the waveforms to occupy. Figure 5.1.2 illustrates the bandwidth and time length expansion of the radar waveform that is used for embedding the communication signals. Here, B and T are the notional bandwidth and time length of the transmitted radar waveform, respectively, while ΔB is the expanded bandwidth and ΔT is the expanded time length used for the communication waveforms. When the

correct length of the radar waveform is used, the blue section on the left side can be used for the communication waveforms, with the red section being occupied by the radar. By using a longer waveform, the blue section on the right can also be used as more space for communication, but the green section is occupied by the extended clutter of the radar and is unavailable. It appears that there would be a trade-off between the extra bandwidth used versus the length of waveform used while maintaining the same SER, but at least some amount of bandwidth expansion is necessary.

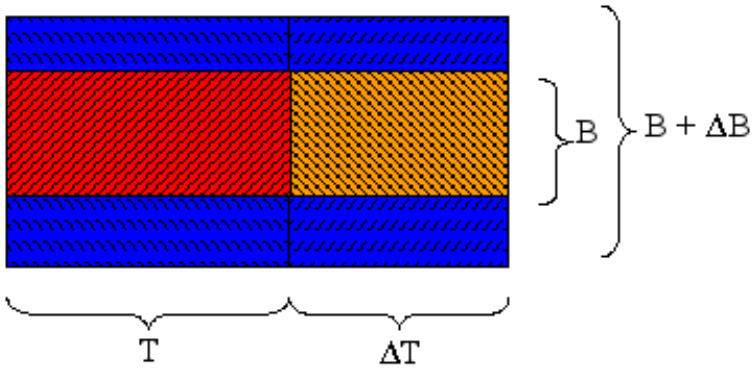

Figure 5.1.2: Illustration of the expansion of time width and bandwidth of the ambient radar scattering.

5.1.3 TEMPORAL AND BANDWIDTH EXPANSION TRADE-OFF

As discussed in the last section, it appears that a trade-off can be made between expanding the bandwidth and extending time length of the radar waveform used in the generation of the communication waveforms while maintaining similar SER performance. To determine the trade-off, 10,000 Monte Carlo simulations are run for each of $M = 1.6, 1.8, 2.0, 2.2, 2.4$ and $\tilde{N} = 100, 120, 140, 160, 180, 200$. The contour plots of iso-SER performance curves for the percentage increase in time

length ($\Delta T/T$) versus the percentage increase in bandwidth ($\Delta B/B$), where $\Delta T/T=(\tilde{N}-N)/N$ and $\Delta B/B=M-1$ are shown in figure 5.1.3.

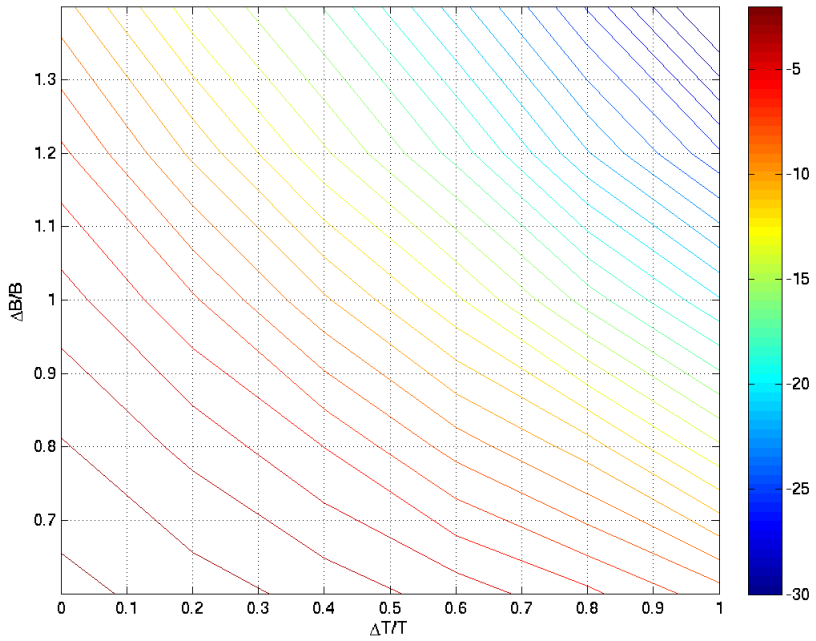

Figure 5.1.3: Iso-SER contours for time width versus bandwidth expansion with -35 dB SIR and -15 dB SNR.

From the illustration in figure 5.1.2, with the blue area designating the space available for the communication waveforms to occupy, the expected rule-of-thumb relationship

$$\Delta B\cdot(T+\Delta T)=\text{constant} \tag{5.1}$$

would represent the trade-off between temporal and bandwidth expansion. This relationship is confirmed by the iso-SER contours shown in figure 5.1.3. Therefore, given a specified value of $(\Delta B)_1/B$ that yields a desired symbol error rate with $(\Delta T)_1/T=0$, the bandwidth can be decreased to $(\Delta B)_2/B$ as long as the time

length is increased to

$$(\Delta T)_2 = T\left[\frac{(\Delta B)_1}{(\Delta B)_2} - 1\right] \tag{5.2}$$

to maintain similar SER performance. Since the embedded communication signal is masked by the bleeding spectrum of the radar waveform and ambient scattering, it is expected that reducing $\Delta B/B$ with the required increase in $\Delta T/T$ will be more LPI (given that the increased time length does not extend past the length of the ambient scattering).

5.2 SYMBOL WAVEFORMS WITH LESS CROSS-CORRELATION

The Dominant-Projection waveform generation approach produces communication waveforms that have about -40 dB pairwise cross-correlation at the match point. Generating communication waveforms that have lower cross-correlation should make the symbol waveforms more separable and possibly improve SER performance. The two methods explored are 1) giving a larger weight to the previously generated waveforms in the projection matrix and 2) adding the Gram-Schmitt approach.

5.2.1 WEIGHTED DOMINANT PROJECTION

With the Dominant-Projection approach, each communication waveform is generated by projecting away the eigenvectors of the dominant space and any previously generated waveform from a random seed vector, known to both the tag and receiver. By giving a larger weight to the previously generated waveforms by

changing equation (2.6) to

$$\mathbf{S}_k = [\mathbf{S}\ a \cdot \mathbf{c}_1 \ldots a \cdot \mathbf{c}_{k-1}] \tag{5.3}$$

where a is the weight value, they will be more prominent in the projection matrix in equation (2.8) and the new waveform will have more of the components in common with the other waveforms projected away. The resulting waveforms will then be less correlated with each other.

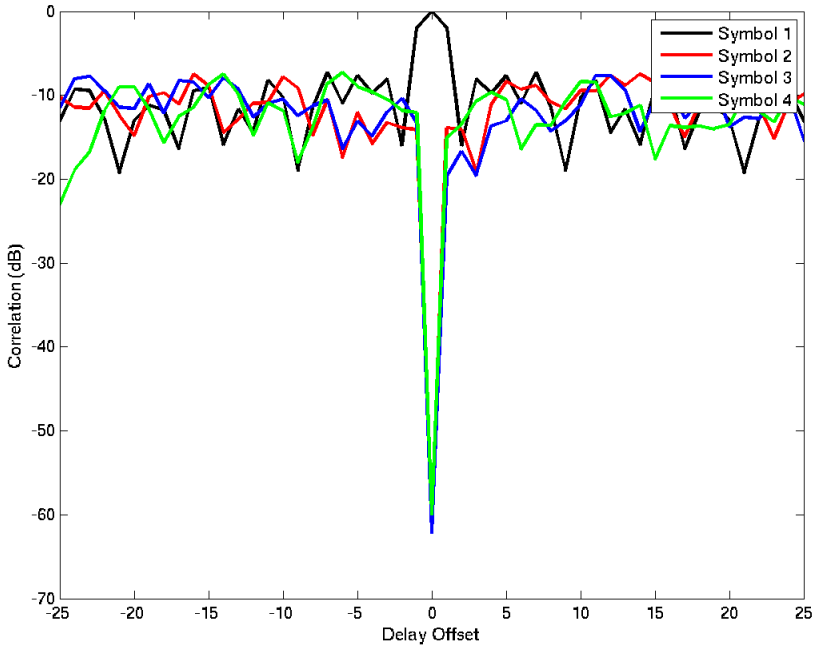

Figure 5.2.1: Cross-correlation of codes with Weighted-Dominant-Projection.

Figure 5.2.1 shows the cross-correlation plots for each of the symbols generated with the Weighted-Dominant-Projection approach with the first symbol waveform. Here we see that the cross-correlation between symbols 2-4 and symbol 1 now drops to below -60 dB at the match point. This is down from the -40 dB seen

with the original Dominant-Projection approach shown in figure 4.3.1. The symbol waveforms are then less correlated with the weighted symbol waveforms.

The SER performance when using the symbol waveforms generated with the Weighted-Dominant-Projection approach is compared with the performance when using the waveforms generated with the original Dominant-Projection approach in figure 5.2.2. From the SER curves, we see that the symbol waveforms with less cross-correlation generated with the Weighted-Dominant-Projection approach do not reduce the probability of symbol error, as the SER performance with the waveforms from both approaches is virtually identical. The reasons for this are explored more in section 5.2.3.

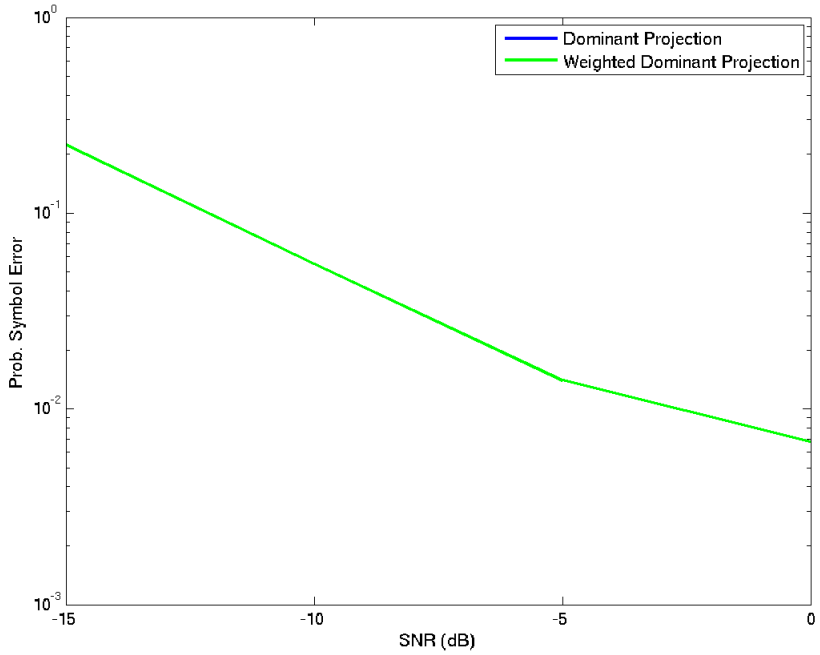

Figure 5.2.2: SER performance of Dominant-Projection and Weighted Dominant-Projection.

5.2.2 DOMINANT-PROJECTION WITH GRAM-SCHMITT

The second method considered for generating communication waveforms that have less cross-correlation is combining the Dominant-Projection approach with the Gram-Schmitt procedure of producing orthonormal vectors. With the Gram-Schmitt procedure [18], a random vector $\mathbf{x}_1$ is selected from the set and normalized as

$$\mathbf{u}_1 = \frac{\mathbf{x}_1}{\left\|\mathbf{x}_1\right\|} \tag{5.4}$$

to generate the first orthonormal vector. A second vector $\mathbf{x}_2$ is then selected from the given set, the projection of $\mathbf{x}_2$ onto $\mathbf{u}_1$ is subtracted out as

$$\acute{\mathbf{u}}_2 = \mathbf{x}_2 - (\mathbf{u}_1^H \mathbf{x}_2)\,\mathbf{u}_1 \tag{5.6}$$

and the result is normalized as

$$\mathbf{u}_2 = \frac{\mathbf{x}_2}{\left\|\mathbf{x}_2\right\|} \tag{5.6}$$

to generate the second orthonormal vector. A third vector $\mathbf{x}_3$ is then selected from the given set, the projection of $\mathbf{x}_3$ onto $\mathbf{u}_1$ and the projection of $\mathbf{x}_3$ onto $\mathbf{u}_2$ are subtracted out as

$$\acute{\mathbf{u}}_3 = \mathbf{x}_3 - (\mathbf{u}_1^H \mathbf{x}_3)\,\mathbf{u}_1 - (\mathbf{u}_2^H \mathbf{x}_3)\,\mathbf{u}_2 \tag{5.7}$$

and the result again normalized to form the third orthonormal vector $\mathbf{u}_3$. This can be repeated to generate orthonormal vectors based on the size of the space that contains the set of vectors $\mathbf{x}_i$.

Since the eigenvectors $\mathbf{V}=[\mathbf{v}_0\ \mathbf{v}_1 \ldots \mathbf{v}_{NM-1}]$ of the correlation matrix $\mathbf{SS}^H$ used in the Dominant-Projection approach are already orthonormal, the Gram-Schmitt procedure can then be used to generate each communication waveform as

$$\mathbf{c}_k=\mathbf{b}_k-\sum_{i=0}^{MN-L}(\mathbf{b}_k^H\mathbf{v}_i)\mathbf{b}_k-\sum_{j=0}^{k-1}(\mathbf{b}_k^H\mathbf{c}_j)\mathbf{b}_k \tag{5.8}$$

where $\mathbf{b}_k$ is the random seed vector known to both the tag and receiver, N is the length of the radar waveform, M is the oversample factor, L is the size of the non-dominant space and $(\cdot)^H$ is the Hermitian operator. Here, the dominant eigenvectors and the previously generated symbol waveforms are directly projected out of the seed vector.

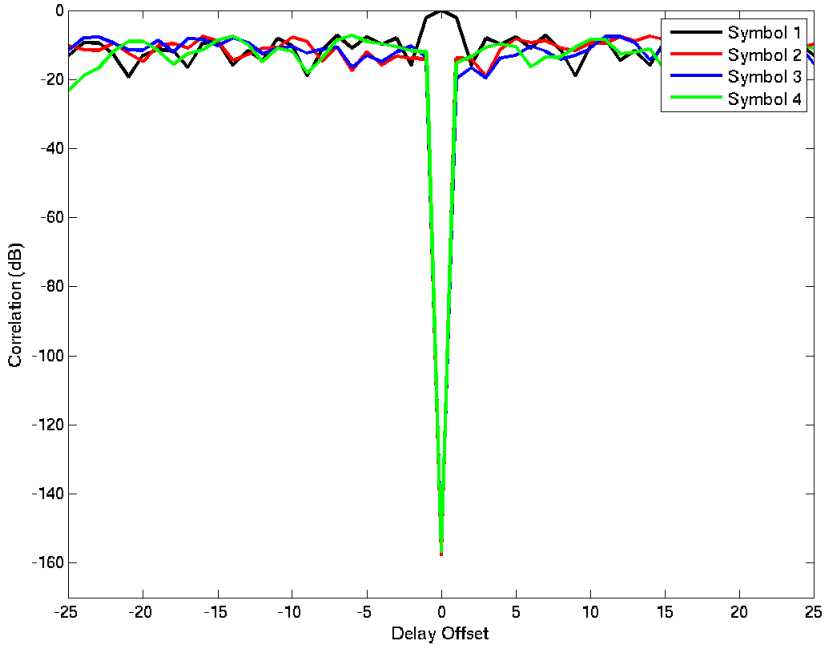

Figure 5.2.3: Cross-correlation of symbol waveforms with Dominant-Projection with Gram-Schmitt.

Figure 3.2.3 shows the cross-correlation plots for the symbol waveforms generated with the combined Dominant-Projection-Gram-Schmitt procedure. In the plots we see that the pairwise cross-correlation is significantly reduced, dropping down to about -160 dB for symbols 2, 3 and 4 with symbol 1.

The SER performance for these new waveforms are compared with the original waveforms in figure 5.2.4. Here, we again see that the communication waveforms with less cross-correlation do not appear to reduce the number of symbol errors. Although it does not improve SER, this procedure does have the computational benefit of only needing to perform one eigen-decomposition instead of one for each symbol required by the Dominant-Projection approach.

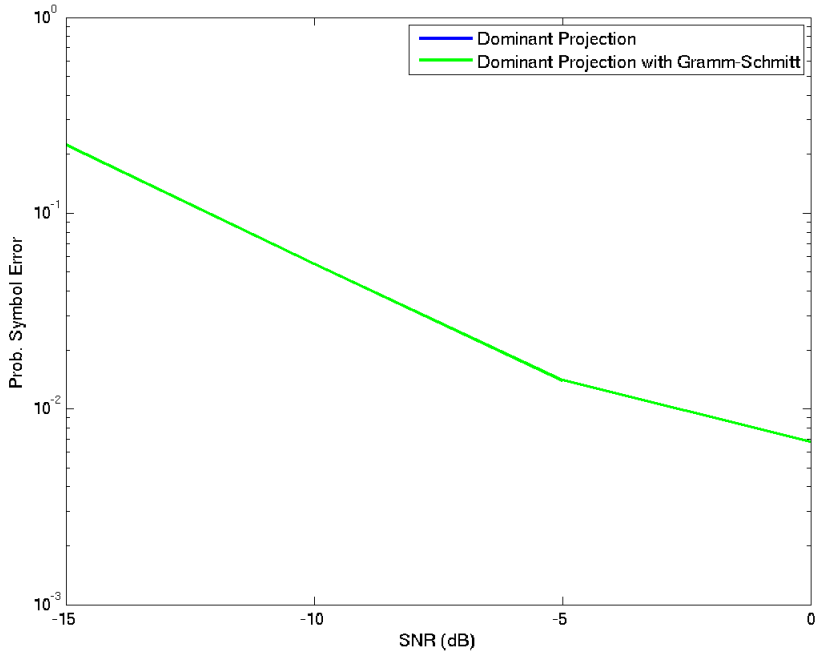

Figure 5.2.4: SER performance of Dominant-Projection and Dominant-Projection with Gram-Schmitt.

5.2.3 FAILURE TO IMPROVE SER

In the last two sections, we saw that generating communication waveforms that have less cross-correlation does not improve SER performance. Although the symbol waveforms are less similar, that does not make them more distinguishable at the receiver. To observe why this is the case, we again look at the probability distribution functions (pdfs) for the output magnitude of the decorrelating filters in the receiver. The estimated pdfs of the filter for the first symbol (which was sent) and the maximum output magnitude of the other three symbols are again generated as in section 4.4. The pdfs for Weighted-Dominant-Projection and the Dominant-Projection-Gram-Schmitt approaches are compared with the original Dominant-Projection approach in figure 5.2.5 below.

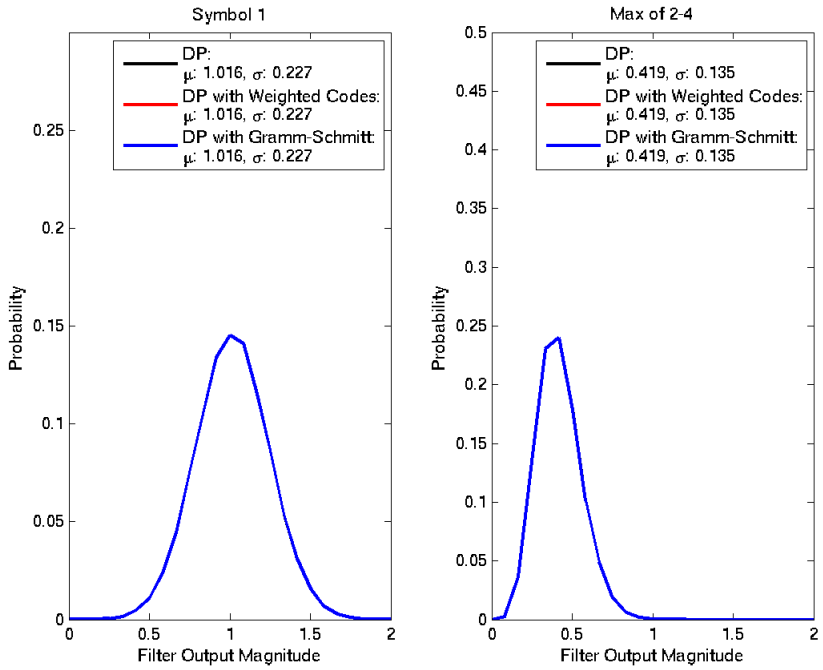

Figure 5.2.5: Estimated pdfs for the communication waveforms with less cross-correlation.

From the plots, we see that both of the new approaches have basically identical probability distributions of the filter outputs. The waveforms with less cross-correlation do not reduce the output magnitude of the maximum of the other three filters or increase the output magnitude of the symbol sent. From these results and the results from section 4.4, it appears that the main contributer to the occurrence of symbol errors is the correlation of each of the symbol waveforms with the interference from clutter. Of course, the communication waveforms are designed to be similar to the clutter in order to remain LPI, so the correlation is intended in the waveform design.

5.3 EQUALIZING INTERFERENCE LEVELS AMONG SYMBOLS

Because the correlation of the communication waveforms with the interference from ambient scattering is a major contributer to symbol error, if the symbol waveforms each have different levels of correlation with the clutter, interference can cause the magnitude of the decorrelating filters for symbols with a higher correlation with the clutter to be larger on average than those with less similarity to the clutter. This unbalance would throw off the probability distributions causing more overlap resulting in more symbol errors.

The correlation of the symbol waveforms with the clutter interference can be equalized by using the Hadamard Transform [19] or some other unitary transformation. This is accomplished by taking a matrix multiplication of the symbol waveforms with a $K \times K$ Hadamard matrix which consists of pairwise orthogonal rows with values $\{-1,+1\}$. The Hadamard Transform mixes the communication

waveforms in order to equalize the correlation of each waveform with the ambient scattering, while still maintaining the pairwise orthogonality of the symbols. An example of a 4×4 Hadamard matrix is

$$\boldsymbol{H}_4=\frac{1}{\sqrt{4}}\begin{Bmatrix}+1 & +1 & +1 & +1\\ +1 & -1 & +1 & -1\\ +1 & +1 & -1 & -1\\ +1 & -1 & -1 & +1\end{Bmatrix}. \tag{5.9}$$

To simulate the effect of equalizing the correlation of the symbol waveforms with the clutter interference by mixing them with the Hadamard Transform, we will use a P3 waveform of length $N=100$ oversampled by a factor of $M=2$. The size of the non-dominant space is $L=64$ with $K=64$ communication waveforms generated such that the entire non-dominant space is used.

The SER performance for this simulation comparing Dominant-Projection approach with and without the Hadamard Transform is shown in figure 5.3.1. From the plots, we observe that the Hadamard Transform does not improve the SER performance for Dominant-Projection. The communication waveforms generated appear to already have an equal interference with the radar clutter without the Hadamard Transform.

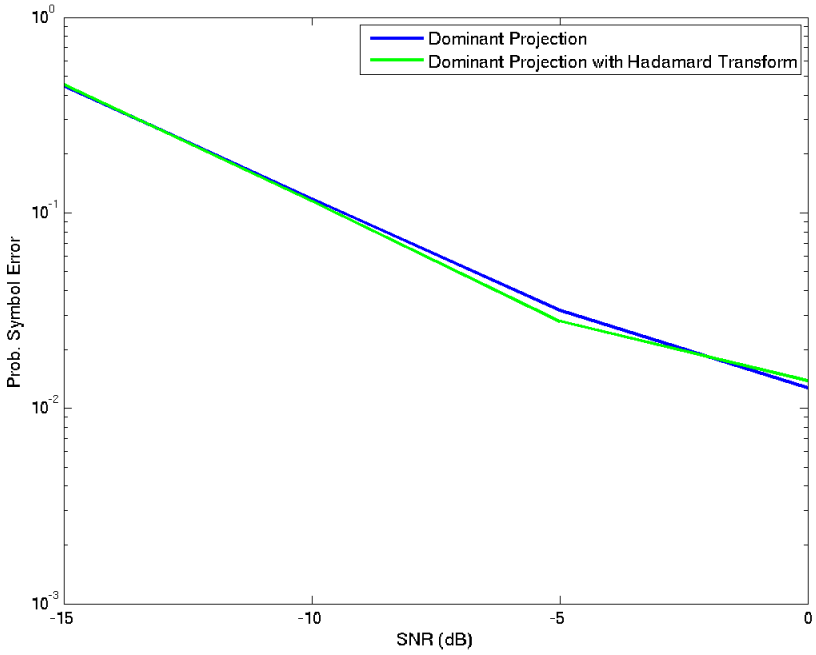

Figure 5.3.1: SER performance of Dominant Projection with the Hadamard Transform.

A situation was found in which the Hadamard Transform did improve the SER performance. If $K=64$ waveforms are generated with the size of the non-dominant space of $L=63$, when the 64th waveform is generated, the entire space for the new communication waveform has already been used. The result is a random signal for the last waveform from residual error from the floating point computation. This random waveform has a higher correlation with the clutter due to the components in common with the dominant eigenvectors and the other waveforms are no longer being projected out. After the Hadamard Transform is applied, the SER performance is significantly improved as seen in figure 5.3.2. This suggests the possibility of generating more symbol waveforms (i.e. $K>L$) by mixing the waveforms generated

with the Dominant-Projection approach with either random or zero vectors. It does show that if a newly developed communication waveform generation approach yields waveforms that have unequal correlation with the clutter, the Hadamard Transformation could be used to equalize the interference.

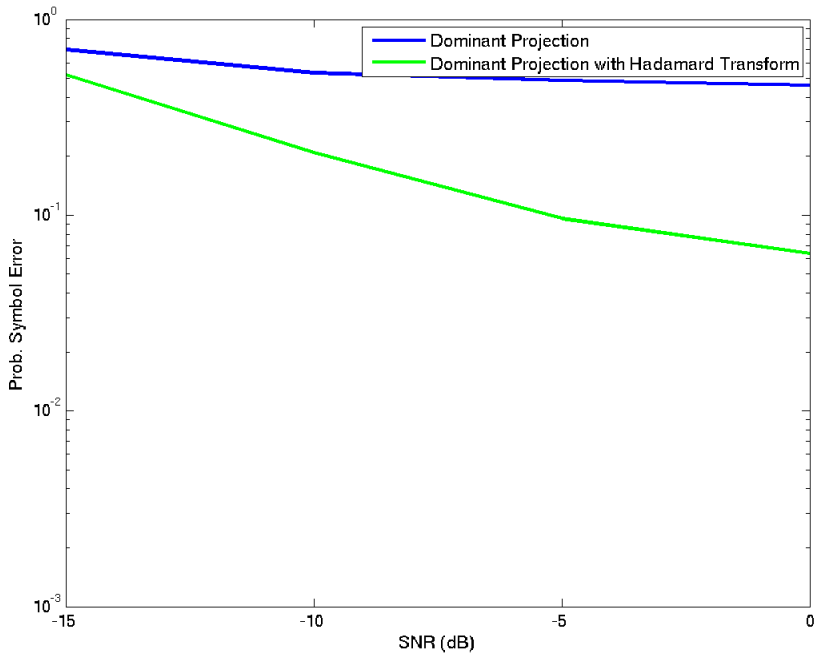

Figure 5.3.2: SER performance of Dominant Projection with the Hadamard Transform equalizing a random symbol.

5.4 ADJUSTING SYMBOL CORRELATION WITH CLUTTER

The amount of correlation between the symbol waveforms and the clutter interference can be adjusted by changing the value used for the size of the non-dominant space L with the Dominant-Projection approach. When L is smaller, more of the dominant eigenvectors will be projected away, making the communication waveforms less like the ambient scattering. With a larger L, less of

the dominant eigenvectors will be projected out, resulting in the waveforms being more similar to the scattering.

The SER performance for $L = 50, 75, 100, 125, 150$ is shown above in figure 5.4.1. In the plot, we see that as expected, larger values of L have a higher probability of symbol error and vice versa. The less similar the symbol waveforms are to the clutter interference, the better the receiver can separate them and the less likely an error will occur.

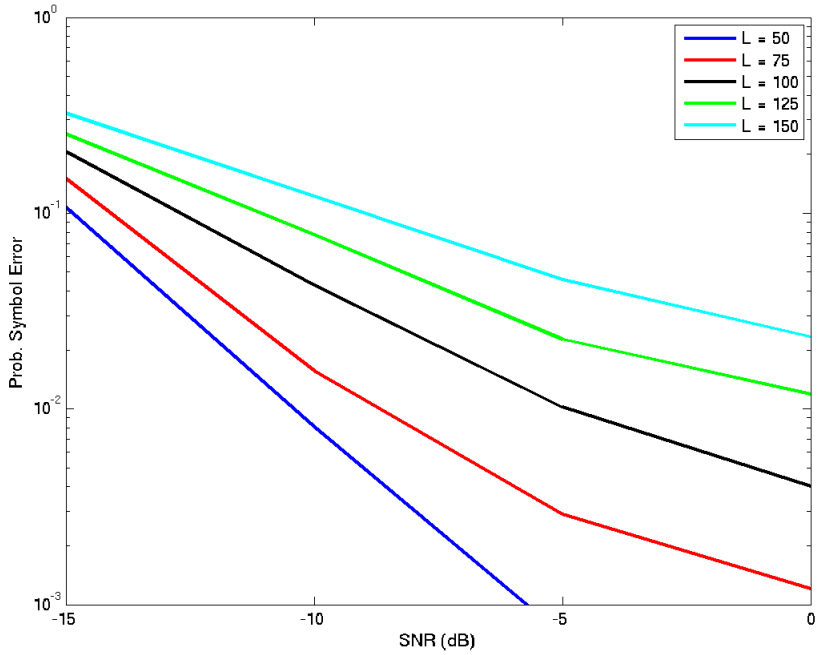

Figure 5.4.1: SER performance when adjusting size of nondominant space.

In figure 5.4.2, we see how the different values of L change the distributions of the decorrelating filter outputs. With a decrease in L, the distribution of the symbol that is present in the received waveform is narrower and taller with a

mean near 1. Also, the maximum of the other three filters has a mean that is reduced with each decrease in L. Less correlation of the symbol waveforms with the ambient scattering lessens the effect of the interference on the distributions of the decorrelating filter output magnitude. The resulting pdfs will have less overlap leading to the improvement in SER performance seen in figure 5.4.2.

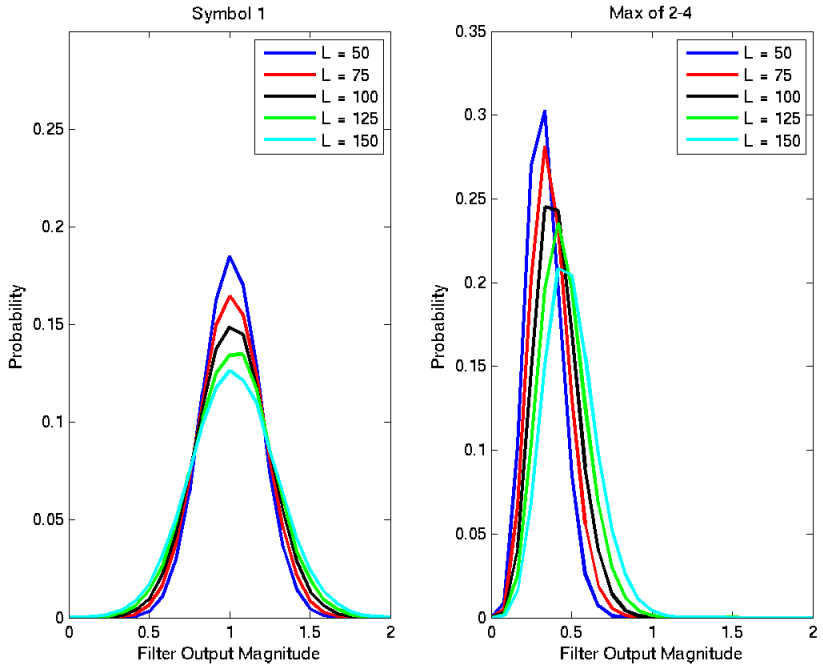

Figure 5.4.2: Changes in estimated pdf from adjusting size of the non-dominant space.

Figure 5.4.3 shows the consequence of reducing the size used for the non-dominant space on the ability of the communication to be covert. When the symbol waveforms are less like the clutter, they will have a greater probability of intercept. From the plot, it is observed that when L is decreased, the LPI metric increases. The SER performance can then be improved by increasing the amount of the

dominant space that is projected out using Dominant-Projection, but improvement comes at the cost of LPI.

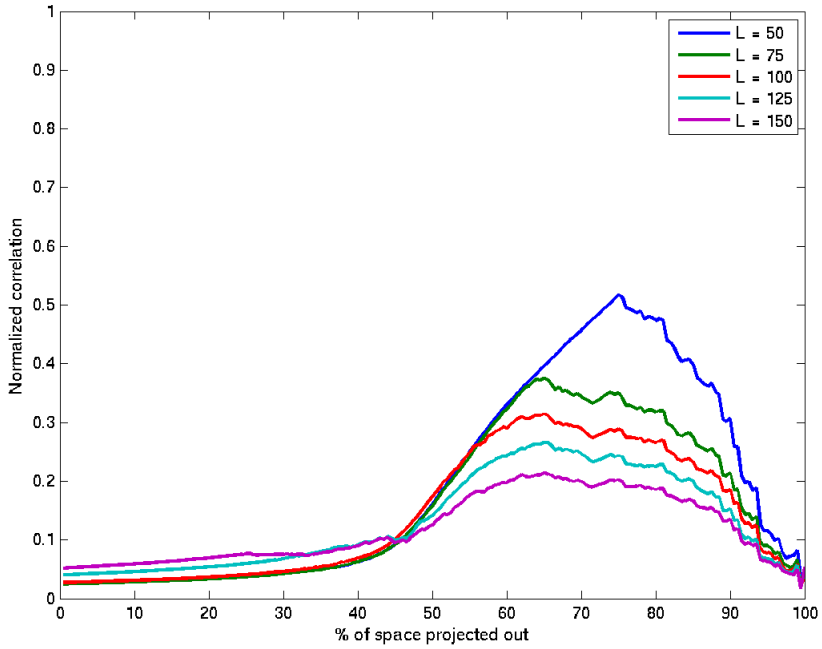

Figure 5.4.3: LPI metric when adjusting the size of the dominant space.

CHAPTER 6

CONCLUSIONS AND FUTURE WORK

This thesis explored some of the real-world aspects of implementing intra-pulse radar-embedded communication. Both the Eigenvectors-as-Waveforms and Weighted-Combining communication waveform generation approaches are sensitive to mismatches in the sampled radar waveform, since each method uses the individual, indexed eigenvectors of the correlation of ambient scattering model generated from the sampled waveform. Multipath distortion, sample rate differences and length variations used for the radar waveform all cause smearing of the eigenvectors, generating mismatched symbol waveforms and resulting in an unusable symbol error rate. The Dominant-Projection approach, on the other hand, uses the eigenvectors of the dominant space as a whole to generate the communication waveforms. Since the smearing of the eigenvectors is mostly contained within the dominant and non-dominant spaces under most of the mismatch scenarios, the approach continues to produce symbol waveforms that are matched, making it robust to the radar waveform mismatches. The probability of symbol error does increase, however, with a lower sampling rate or a shorter length for the radar waveform.

Synchronization is important for intra-pulse radar embedded communication to be effective, as the number of samples over which the receiver must look for the communication waveform from the tag increases the probability of a symbol error. Differing levels of synchronization could be achieved with the receiver having

previous knowledge of the tags location (and thus, time delay) or searching and tracking a moving tag. SER performance would then be dependent on the receiver's ability to track the time delay of the waveform sent by the tag.

Attempts to improve SER performance without perfect synchronization were made by averaging over three samples and generating waveforms with lower local cross correlation, but neither was able to reduce the number of symbol errors in simulations. Also, communication waveforms with less cross-correlation were generated in a failed attempt to make the symbols more separable and decrease the chance of error. The less cross-correlated waveforms and the waveforms with less local cross correlation do not improve SER performance due to the correlation of each symbol with the clutter interference dominating over the pairwise cross-correlation between each symbol waveform.

Adjustments can be made to the Dominant-Projection approach based on the environment. Because each symbol is correlated with the ambient scattering in order for it to be hidden and have a low probability of intercept (LPI), by projecting away more of the dominant eigenvectors the communication waveforms will be less correlated with the clutter interference. This will decrease the probability of symbol error, but increase the probability of intercept. The time length of the radar waveform can be increased in addition to the bandwidth expansion for added dimensionality in the generation of the communication waveforms. The longer resulting symbol waveforms are easier for the intended receiver to separate from the interference and noise, but still remain hidden due to the extended length of the clutter interference.

The bandwidth used for the communication waveforms could also be decreased when increasing the waveform length to retain the same SER performance. This trade-off would result in more LPI communication with less bandwidth used outside the radar as long as the longer waveform does not extend past the length of the ambient scattering.

FUTURE WORK

1. Only the output magnitude of the decorrelating filter is used in the receiver. The phase of the output may be used as an extra dimension to encode data (as in M-PSK) or as a way to differentiate the signal from the noise.

2. Simulations to this point have assumed that there is always a communication signal present. Further work is needed for detecting whether a symbol is present in the backscatter (inclusion of the null set). The probability distribution functions from chapter 4 could be used as a starting point for setting a detection level, but requires calibration based on the power level of the communication waveform at the receiver.

3. So far, only one symbol waveform has been sent by the tag at a time. With the waveforms being orthogonal, more than one waveform could be sent by the tag and detected at the receiver at one time, similar to CDMA or at different dleays. Being able to send multiple waveform could be used as a way to encode more bits for a higher data rate or to aid in detection (some number of waveforms must be detected to determine a symbol was present).

4. The convolutional coding method for intra-pulse communication should be compared with the Dominant-Projection approach in terms of symbol error rate performance and the probability of intercept.

5. More work is needed to improve performance of the receiver when the symbol waveforms encounter multipath distortion from the tag.

6. The tag using convolution coding may be combined with intra-pulse phase changed to provide masking interference as well as registration for the receiver.

7. Develop a communication waveform generation approach that is less computationally intensive than the Dominant-Projection approach (i.e. a method that does not require an eigen-decomposition).

References

[1] S.D. Blunt and P. Yatham, “Waveform design for radar-embedded communications”, *3rd International Waveform Diversity and Design Conference*, pp. 214-218, Pisa, Italy, June 4-8, 2007.

[2] S.D. Blunt, P. Yatham, and J. Stiles, “Intra-pulse radar embedded communications,” to appear in *IEEE Trans. Aerospace & Electronic System*.

[3] S.D. Blunt, J. Stiles, C. Allen, D. Deavours, and E. Perrins, "Diversity aspects of radar-embedded communications," proc. of *Intl. Conf. on Electromagnetics in Advanced Applications*, Sept. 17-21, 2007.

[4] S.D. Blunt and C.R. Biggs, “Practical Considerations for Intra-Pulse Radar-Embedded Communications”, *4th International Waveform Diversity and Design Conference*, pp. 244-248, Orlando, FL, February 8-13, 2009.

[5] S. Kingsley and S. Quegan, *Understanding Radar Systems*, SciTech Publishing, Inc., 1999.

[6] H. Stockman, “Communication by Means of Reflected Power” *Proceedings of the IRE*, October 1948, pp. 1196-1204.

[7] R.M. Axline, G.R. Sloan, and R.E. Spalding, "Radar Transponder Apparatus and Signal Processing Technique," US Patent 5,486,830, 23 Jan 1996.

[8] D. Hounam and K.H.Wagel, "A technique for the identification and localization of SAR targets using encoding transponders," *IEEE Trans. Geoscience and Remote Sensing*, vol. 39, no. 1, pp. 3-7, Jan. 2001.

[9] D.L. Richardson, S.A. Stratmoen, G.A. Bendor, H.E. Lee, and M.J. Decker, "Tag Communication Protocol and System," US Patent 6,329,944, 11 Dec 2001.

[10] R.M. Axline, G.R. Sloan, and R.E. Spalding, "Transponder Data Processing Methods and Systems," US Patent 6,577,266, 10 Jun 2003.

[11] R.C. Ormesher and R.M. Axline, "Methods and system suppressing clutter in a gain-block, radar-responsive tag system" US Patent 7,030,805, 18 Apr 2006.

[12] J.J. Komiak, D.A. Barnum, D.E. Maron, “Digital RF tag,” US Patent #7,106,245, issued Sept. 12, 2006.

[13] R.C.Dixon, Spread Spectrum Systems, New York: John Wiley& sons, Inc., 1976.

[14] S. Verdu, *Multiuser Detection*, Cambridge University Press, Cambridge, UK, 1998.

[15] R. Lupas and S. Verdu, "Linear multiuser detectors for synchronous code-division multiple-access channels," IEEE Trans. Information Theory, vol. 35, pp. 123-136, Jan. 1989.

[16] B. L. Lewis and F. F. Kretschmerm, “Linear Frequency Modulation Derived Polyphase Pulse Compression Codes”, *IEEE Trans. Aerospace and Electronic Communications, Vol AES 18, No 5*, Sept 1982, pp. 637-641.

[17] S.D. Blunt and K. Gerlach, "Adaptive Pulse Compression via MMSE Estimation," *IEEE Trans. Aerospace & Electronic Systems,* vol. 42, no. 2, pp. 572-584, April 2006.

[18] J. G. Proakis and Masoud Salehi, *Digital Communications*, Fifth Edition, McGraw-Hill, 2008.

[19] G. L. Stüber, *Principles of Mobile Communication*, Second Edition, Kluwer Academic Publishers, 2001.